AGU PUBLICATIONS

Global Biogeochemical Cycles

RESEARCH ARTICLE
10.1002/2016GB005478

Key Points:
- First zonal and vertical measurements of soluble, dissolved, and particulate cobalt over the entire Mediterranean Sea
- High-surface external inputs, biological uptake, scavenging, circulation, and mixing govern the DCo distribution in the Mediterranean Sea
- Anthropogenic activities impact the Mediterranean Co distribution, but tentative Co budgets were balanced at basin scale

Supporting Information:
- Supporting Information S1

Correspondence to:
G. Dulaquais,
gabriel.dulaquais@univ-brest.fr

Citation:
Dulaquais, G., H. Planquette, S. L'Helguen, M. J. A. Rijkenberg, and M. Boye (2017), The biogeochemistry of cobalt in the Mediterranean Sea, *Global Biogeochem. Cycles*, *31*, 377–399, doi:10.1002/2016GB005478.

Received 8 JUL 2016
Accepted 31 JAN 2017
Accepted article online 2 FEB 2017
Published online 24 FEB 2017

The biogeochemistry of cobalt in the Mediterranean Sea

Gabriel Dulaquais[1], Hélène Planquette[1], Stéphane L'Helguen[1], Micha J. A. Rijkenberg[2], and Marie Boye[1]

[1]Laboratoire des Sciences de l'Environnement Marin CNRS UMR 6539, Institut Universitaire Européen de la Mer, Université de Bretagne Occidentale, Plouzané, France, [2]NIOZ Royal Netherlands Institute for Sea Research, Department of Ocean Systems, Utrecht University, Den Burg, Netherlands

Abstract The soluble (sCo < 0.02 μm), dissolved (DCo < 0.2 μm), colloidal (cCo, as DCo minus sCo), and the particulate (pCo > 0.2 μm) fractions of cobalt were investigated along the GEOTRACES-A04 section. Our results show that sCo was the predominant form (90%) of the DCo in the Mediterranean Sea and that cCo and pCo generally followed the same distribution, suggesting a biogeochemical link between these two fractions. In the Mediterranean Sea, DCo displayed an overall scavenged-like profile in the different sub-basins, with high concentrations (up to 350 pM) in surface and quasi-uniformed low concentrations of DCo (~45 pM) in the deep sea. However, the decoupling between the surface and the deep reservoirs suggested that the transfer of Co from dissolved to particulate pools during the sink of particles may not be the only process governing DCo distribution. High-surface Co inputs, stabilization of DCo in a soluble form, and the extremely high regeneration rate of biogenic pCo all lead to the accumulation of DCo in surface. Conversely, low pCo export from the surface waters, low remineralization of biogenic pCo, and slow but efficient removal of DCo by scavenging including colloid aggregation into particles prevented its accumulation in the intermediate and deep sea. Moreover, Mediterranean circulation prevented the exchanges between the DCo-rich surface and the DCo-poor deep layers enhancing the scavenged-like profile of DCo. Finally, tentative DCo budgets were balanced at basin scale and showed the strong imprint of the surface inputs at Gibraltar Strait on the Mediterranean cobalt biogeochemistry.

1. Introduction

Cobalt (Co) is a key element for marine life. It is the central atom of the B_{12} vitamin, a biomolecule used in several biological pathways [*Raux et al.*, 2000; *Martens et al.*, 2002]. B_{12} abundance is suspected to play a role in phytoplankton growth, productivity, and diversity [*Sañudo-Wilhelmy et al.*, 2006; *Panzeca et al.*, 2006; *Bertrand et al.*, 2007; *Gobler et al.*, 2007], and Co availability could be a key factor regulating the biosynthesis pathway of this vitamin [*Panzeca et al.*, 2008]. Moreover, Co can be substituted for zinc or cadmium as cofactor in carbonic anhydrase and likely in alkaline phosphatase [*Price and Morel*, 1990; *Sunda and Huntsman*, 1995; *Yee and Morel*, 1996; *Lane and Morel*, 2000; *Lane et al.*, 2005; *Gong et al.*, 2005], two enzymes involved in the acquisition of inorganic carbon and phosphate, respectively. The cyanobacteria *Synechococcus* and *Prochlorococcus* are known to primarily require Co for their growth [*Sunda and Huntsman*, 1995; *Saito et al.*, 2002], and they can represent an important part of the primary production in oligotrophic waters [*Goericke and Welschmeyer*, 1993]. Thus, primary production can be significantly cobalt-dependent in oligotrophic marine systems. In the oligotrophic Mediterranean Sea (MS), which is known to be one of the least productive marine systems of the world [*Bethoux et al.*, 1998, 2002], and particularly sensitive to anthropogenic forcing even at short time scales [*MerMex group*, 2011], the cyanobacteria *Synechococcus* and *Prochlorococcus* represent a high proportion of the biomass [*Ignatiades et al.*, 2009; *van de Poll et al.*, 2015], thereby enhancing the biological utilization of Co. Moreover, elevated B_{12} surface concentrations recorded in the MS were linked, among others, to high surface dissolved cobalt (DCo) concentrations [*Bonnet et al.*, 2013], further suggesting that Co is a key parameter of the Mediterranean ecosystem.

Despite these indirect evidences on the biological importance of Co, its biogeochemistry is poorly documented in the MS. Previously reported DCo surface concentrations are elevated compared to other oligotrophic domains and increase eastward from the Western Basin to the Aegean Sea [*Tovar-Sánchez et al.*, 2014]. Atmospheric inputs and Gibraltar Strait surface fluxes are thought to be the main sources and scavenging to be the main sink of DCo [*Zhang et al.*, 1989; *Guieu et al.*, 1997; *Elbaz-Poulichet et al.*, 2001a, 2001b]. In addition, other external inputs such as submarine ground water discharge and riverine inputs might also be sources of

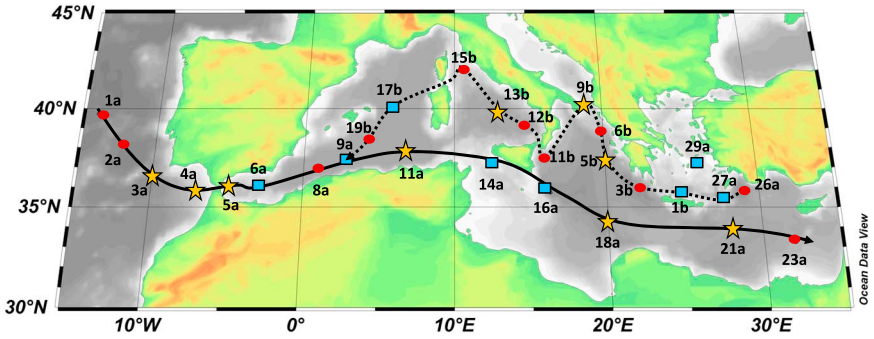

Figure 1. Sampling locations along the GAO4N section. Red dots: sampling for dissolved cobalt (DCo) only; blue squares: sampling for DCo, particulate trace elements (PTEs), and particulate nutrients (PNs); yellow stars: sampling for DCo, PTE, PN, and soluble cobalt. The filled and dashed lines indicate the southern and northern routes of the cruise track that are referred in other figures.

Co to the MS [*Elbaz-Poulichet et al.*, 2001b; *Rodellas et al.*, 2015]. Full-depth scavenged-type profiles of DCo with local maxima close to the bottom were reported in the Western Basin, but data remain scarce and scattered [*Ngoc and Whitehead*, 1986; *Zhang et al.*, 1989; *Morley et al.*, 1997; *Heimbürger et al.*, 2011], while the distribution of DCo in the Eastern Basin is actually unknown. Moreover, all the previous DCo analyses were performed on non-UV-treated samples, likely leading to underestimated concentrations [*Vega and van den Berg*, 1997]. Furthermore, to our knowledge, there is actually no published data of the size partitioning of DCo between the soluble and the colloidal fractions and there is also no available data of Co in suspended particles in the MS. As a result, many questions on the Mediterranean biogeochemical cycle of this bioessential element remain unresolved.

The purpose of this study is to design a synoptic view of the biogeochemistry of Co in the MS. To this aim, we investigated the zonal and vertical distributions of DCo and particulate Co (pCo) in the different sub-basins of the MS, with the exception of the Adriatic Sea and the Northwestern Basin. Here we report the most comprehensive DCo data set and the first measurements of particulate and soluble Co in the MS, along the GEOTRACES-A04 section (Figure 1). We used these data to identify the main sources, sinks, and processes governing the surface and the deep water distribution of cobalt and finally propose a DCo budget at basin scale.

2. Methods

2.1. Cruise Track and Sampling

Samples were collected aboard the Dutch R/V *Pelagia* along the GEOTRACES-A04N section (Figure 1) spreading from the Northeast Atlantic (14.2°W, 39.7°N) to the Marmara Sea (27.5°E, 40.8°N). The first cruise (64PE370, Leg 1) was conducted from 14 May to 5 June 2013 and the second (64PE374, Leg 2) from 25 July to 11 August 2013. A total of 56 stations were sampled for phosphates (PO_4^{3-}), 29 stations for DCo among which 9 stations were subsampled to investigate the partitioning between soluble (sCo) and colloidal (cCo) cobalt. In addition, 17 stations were sampled for particulate trace elements (Co, P, Mn, Al, and Fe) and 10 for surface particulate organic carbon and nitrogen determination. The locations of the sampling stations are shown in Figure 1. All samples were collected by using the TITAN conductivity-temperature-depth (CTD) frame of Nederlands Instituut voor Onderzoek der Zee (NIOZ, Netherlands), with 24 ultra-clean sampling PRISTINE bottles of 24 L each made of polyvinylidene (PVDF) and titanium [*Rijkenberg et al.*, 2015]. After deployment the TITAN system was moved to a Class 100 container for subsampling [*de Baar et al.*, 2008]. Here all 100 samples were collected by using inline filtration under N_2 pressure (filtered 99.99% N_2, 0.7 atm).

Seawater was filtered through 0.2 μm Sartobran 300 cartridges (Sartorius) for DCo analyses and collected in acid-cleaned 250 mL low-density polyethylene (LDPE) Nalgene® bottles. At selected stations, sCo samples were collected in acid-cleaned 60 mL LDPE Nalgene® bottles by connecting a 0.02 μm Virosart CPV MidiCaps Sartorius cartridge inline to the 0.2 μm Sartobran 300 cartridge. Before collection, acid-cleaned sample bottles were rinsed 5 times with sample seawater. All seawater samples were then acidified by using ultrapure® HCl at 0.01 M (Merck) within an hour after their collection. Finally, the acidified samples were stored

double bagged in the dark and ambient temperature until analyses (2–3 months after collection) in the shore-based laboratory.

Particulate trace elements were collected after filtration of 4 to 15 L of seawater through 47 mm diameter polyester sulfone filters 0.22 μm pore size (PES, Supor) mounted with Teflon pliers on Teflon filter holders (47 mm, Savillex). Filter holders were connected inline to the PVDF samplers. Prior to sampling, the entire sampling equipment used to collect particles was acid cleaned by using 0.1 M Suprapur® HCl (Merck) and subsequently rinsed with sample seawater. Immediately after filtration, filters were stored at −20°C in double-bagged acid-cleaned and dried PetriSlides® (Millipore). All filters were acid cleaned following the method of *Planquette and Sherrell* [2012] and stored in a Teflon beaker filled with ultrapure water (18.2 MΩ cm, Millipore). Process blank filters were systematically collected at every sampling station as described in *Planquette and Sherrell* [2012], for a deep (typically 1500 m) and a surface sample (50 m). To this aim, the Teflon filter holder was connected to the filtration cartridge (0.2 μm, Sartobran® 300). The standard volumes for these flow-through blanks were 10 L and 5 L, respectively, for deep and surface waters.

Particulate organic carbon and nitrogen samples were collected after inline filtration of seawater (1 to 2 L) through 47 mm precombusted (450°C, 4 h) Whatman GF/F filters mounted onto acid-cleaned polyethylene sulfone filter holders. Prior to collection, acid-cleaned filter holders were rinsed with seawater samples. Process flow-through blanks (1 L) were sampled following the same procedure as described for particulate trace elements. The GF/F filters were then stored at −20°C in precombusted receptacles.

2.2. Hydrography and Phosphate Analysis

The hydrological parameters (salinity (S), temperature, dissolved oxygen (O_2), and fluorescence) were measured by using an SBE911+ CTD system. PO_4^{3-} samples (unfiltered) were collected in 125 mL polypropylene bottles and were typically analyzed within 18 h on a Seal Analytical QuAAtro autoanalyzer following the colorimetric methods of *Grasshoff et al.* [1983] for PO_4^{3-}. Accuracy and precision of the measurements were assessed by measuring an in-house mixed nutrient standard and the reference material (Reference Material for Nutrients in Seawater (RMNS), lot BU) supplied by KANSO (Japan). Reproducibility of the method was better than 1%, and nutrient concentrations measured for the RMNS were in agreement with consensus values.

2.3. Determination of Dissolved and Soluble Cobalt

Prior to analyses, the DCo and sCo samples were UV-oxidized for 3 h in acid-cleaned silica tubes with Teflon caps, using a high-pressure mercury vapor lamp [*Dulaquais et al.*, 2014a]. The samples were then analyzed within 24 h by flow injection analysis and chemiluminescence detection following the method described in *Dulaquais et al.* [2014a]. Briefly, analytical reagents were prepared by using high-purity Milli-Q water and trace metal quality reagents under a laminar flow hood (ADS Laminaire, International Organization for Standardization 5 class). All reagents were prepared daily and stored overnight to allow temperature equilibration before analysis. Due to the wide range of DCo concentrations, the samples collected below 500 m and above 500 m were calibrated against a 6-point calibration curve made with standard additions up to respectively 120 pM and 400 pM of cobalt added to artificial and Chelex-cleaned seawater. Calibrations were run before and after each series of 8 to 12 samples which included a duplicate sample spiked with 50 pM of cobalt. For blank correction, two reagent blanks were analyzed in acidified deionized water at the beginning and at the end of each series [*Bown et al.*, 2011; *Dulaquais et al.*, 2014a]. The samples were measured in triplicate, and the mean peak heights corrected for the blanks were used to estimate the concentrations. The final standard error (SE) of the measurement is calculated by an error propagation by using the errors on blanks, the calibration curves, and the deviation of the triplicate analyses. Small colloidal Co concentrations (cCos) were calculated by subtraction of sCo from DCo. cCo was operationally defined in this study as the DCo between 0.02 μm and 0.2 μm. The standard deviation of cCo was determined by following equation (1). Pair *t* test was performed between sCo and DCo data sets in order to ensure that the two data sets were significantly different. The results indicate that cCo data set can be used with 95% confidence ($p < 0.05$, *t* value = 8.52, and critical *t* value = 1.98).

$$\mathrm{SEcCo} = \sqrt{(\mathrm{SEDCo})^2 + (\mathrm{SE\ sCo}^2)} \quad (1)$$

where SE DCo and SE sCo are the standard deviations of DCo and sCo measurements, respectively.

The mean reagent blank (based on all blank determinations) for sCo and DCo was 4.4 ± 1.8 pM (n = 87). The limit of detection of the method which was defined as 3 times the standard deviation of the mean reagent blank was therefore 5.4 pM. Before each series of samples, the accuracy of the calibration curve was checked by analyzing one reference sample collected during SAFe program or the GEOTRACES program. These reference samples were UV-digested and analyzed following the same protocol as our samples. The mean DCo concentration values measured in SAFe S and D1 and in surface reference and deep reference samples were 5.1 ± 2.2 pM, 42.3 ± 1.4 pM, 29.8 ± 2.0 pM, and 63.2 ± 2.3 pM, respectively. These results are in excellent agreement with the consensus values (see more details in Table S1 in the supporting information). Finally, the analytical precision of the method was determined from repeated analyses of the same sample collected at 1000 m depth in the Central MS (station 11a), yielding an uncertainty of ±2.1%, expressed as relative standard deviation on the mean (DCo = 47.4 ± 1.0 pM; n = 10).

2.4. Determination of Particulate Trace Element Concentrations

The particles collected onto PES filters were digested, following the procedure described in *Planquette and Sherrell* [2012]. Manipulations were performed within a class 100 clean hood. The filters were placed alongside the walls of rounded bottom screw cap Teflon PFA vials (30 mL, Savillex®), wherein 3 mL of an acid solution was added (HNO_3 8 M, Merck Ultrapur®; HF 2.9 M, Merck Suprapur®). The vials were then closed and heated at 130°C on a Teflon thermostated plate during 4 h in a Class 100 all plastic fume hood. After a cooling step, the vials were opened and heated at 110°C to evaporate the acid solution to near dryness. Then, the residual filters were removed and 6 mL of 0.8 M HNO_3 solution spiked with indium (1 ppb) and rhenium (10 ppb), used as drift monitor, was introduced in the vials and then transferred into acid-cleaned 15 mL polypropylene tubes (Corning®) for archiving before analysis.

Trace element analyses were performed on a sector field inductively coupled plasma–mass spectrometry element 2 (Thermo). In this study, only the low resolution mode for Cd and Pb and medium resolution for other element were used. On the day of analysis, 500 μL of archived solution was diluted with 3 mL of HNO_3 (0.8 M, ultrapure Merck) solution in acid-cleaned polypropylene tubes (Corning®). Every eight samples, a replicate as well as a tube blank were prepared. Given the variability of concentration range and elemental ratios in the environment, two multielemental solutions were prepared from single-element primary standard solutions. All working solutions for calibration were prepared gravimetrically from 10 or 1000 mg L^{-1} National Institute of Standards and Technology traceable primary standards purchased from high purity standards and diluted to appropriated concentrations with 0.8 M HNO_3, ultrapure Merck. To avoid potential cross contamination when mixing high- and low-concentration standards, two separate multielement standard curves were constructed: one with high concentration for Al, P, Ca, Fe, Sr, and Ba and another with low concentrations for Ti, V, Cr, Mn, Co, Ni, Cu, Zn, Cd, Mo, Pb, and Zr. The two 10-point external standard curves were prepared from multielement mixed standard stock solutions spiked with Indium (1 ppb). The ranges of the calibration curves covered 2 orders of magnitude of the expected range in the environmental samples and were run at the beginning, the middle, and the end of each sequence. Reproducibility of the method was determined by rerunning the same sample after each series of eight samples. The reproducibility for each element was always $<$10%. Flow-through process blanks were respectively 4599, 4413, 323, 2172, 902, and 8.15 pmol per filter for Al, P, Mn, Fe, Ti, and Co. Accuracy was checked with certified reference material Bureau of Reference 414a (see Table S2).

2.5. Determination of Particulate Organic Nitrogen and Carbon Concentrations

Before analysis, the filters were placed in a desiccator with fuming HCl Normapur (10 N, Merck) during 4 h to eliminate the inorganic phase. After that, the filters were dried in an oven for 24 h (60°C). Particulate organic carbon (POC) and particulate organic nitrogen (PON) concentrations were quantified by using a mass spectrometer (Delta+, ThermoFisher Scientific) coupled to a C/N analyzer (Flash EA, ThermoFisher Scientific) via a type III interface. The limits of detection, estimated as 3 times the standard deviation of the mean reagent blank, were on average 0.51 and 0.06 μmol L^{-1} for POC and PON concentrations, respectively.

3. General Hydrography

3.1. Eastern Atlantic and Gibraltar Strait

Surface waters (0–200 m) in the Eastern Atlantic were relatively salty and less dense than the underlying North Atlantic Central Water (NACW) (Figure 2a). NACWs, mostly composed of Antarctic Intermediate

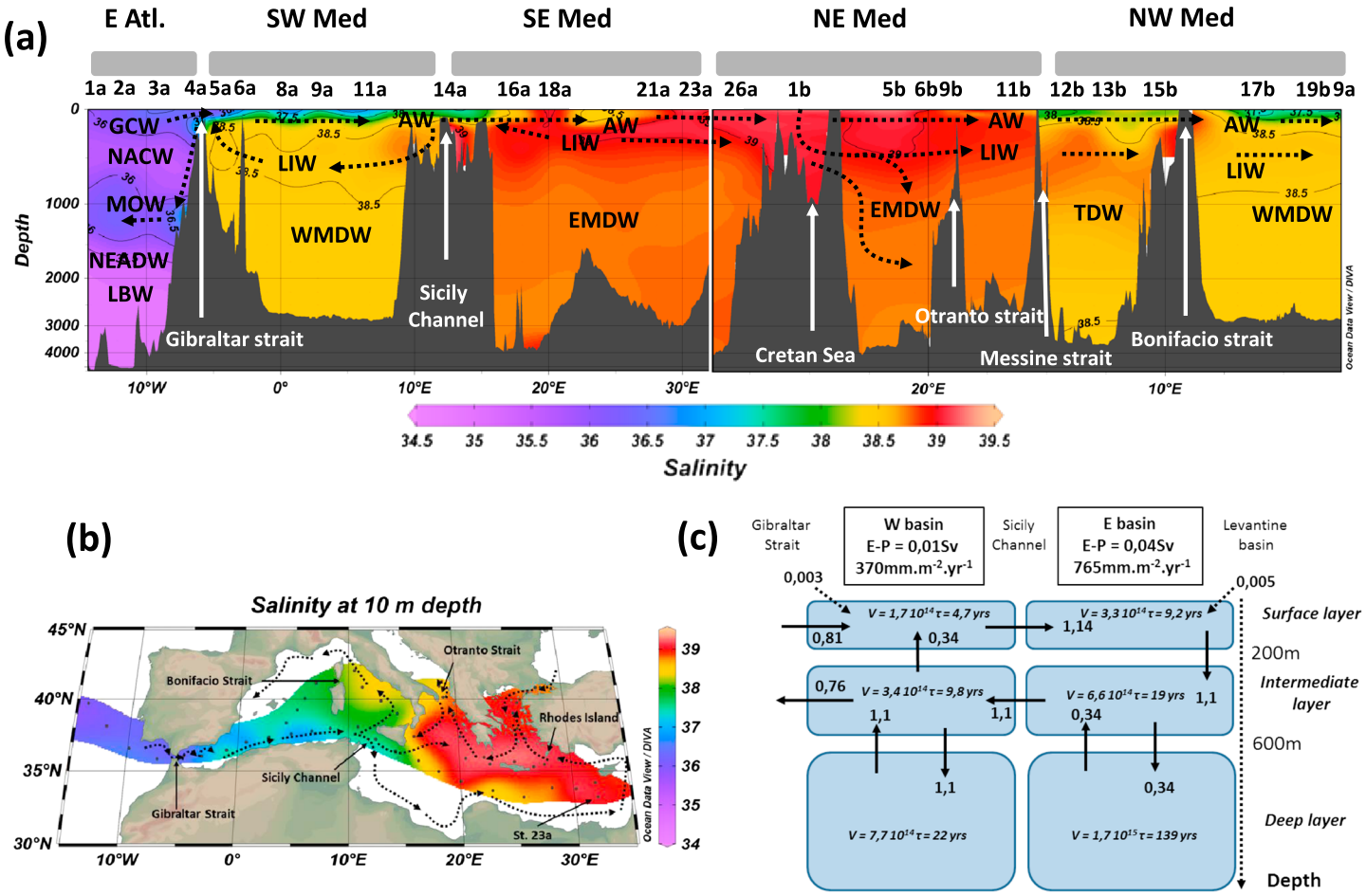

Figure 2. (a) Vertical and spatial salinities along the (left) southern and (right) northern routes of the section referred in Figure 1, where water masses are labeled (see text for definitions and abbreviations). (b) Spatial distribution of salinity at 10 m depth. The dashed arrows indicate the Mediterranean circulation in the intermediate and deep reservoir (Figure 2) and in surface waters (Figure 2b). (c) Conceptual hydrological model, with the volume and residence time for the different layers used in this study. All water fluxes are given in Sverdrup ($1\ Sv = 10^6\ m^3\ s^{-1}$, after *Astraldi et al.* [1999], *Bethoux* [1980], *Durrieu de Madron et al.* [2013], *Lascaratos et al.* [1999], *Mariotti et al.* [2002], *Manzella et al.* [1988], *Roether and Schlitzer* [1991], *Soto-Navarro et al.* [2010], *Struglia et al.* [2004], *van Cappellen et al.* [2014], and *Zervakis et al.* [2004]).

Water (AAIW), were flowing northward across the Eastern Atlantic and were located between 400 and 750 m (Figure 2a). This water mass has a lower salinity (Figure 2a) [*Tsuchiya et al.*, 1992] than the underlying Mediterranean Outflow Water (MOW) centered at 1000 m (Figure 2a). The upper MOWs (750–1000 m) are mixed with the AAIW and the lower MOW (1000–1250 m) with the Labrador Seawater (LSW). Similarly to NACW, MOWs are transported across the Atlantic Ocean with the AAIW [*van Aken*, 2000b]. The Northeastern Atlantic Deep Waters (NEADWs) were observed between 1500 and 2500 m. Below 2500 m, the Lower Deep Waters (LDWs) are mixed with Antarctic Bottom Water (AABW) and follow a northward pathway [*Mantyla and Reid*, 1983; *McCartney*, 1992; *Schmitz and McCartney*, 1993].

Although water fluxes reported at Gibraltar Strait vary depending on the study (see review of *Ribera d'Alcalà et al.* [2003]), most studies give similar estimates for the net water inflow. Indeed, the net inflow has been estimated to be 0.057 ± 0.009 Sv ($1\ Sv = 10^6\ m^3\ s^{-1}$ [*Boutov et al.*, 2014]) and it balances the net evaporation rate of 50–100 cm yr^{-1} in the MS (Figure 2c [*Mariotti et al.*, 2002]). The Atlantic Waters (AWs) enter the MS via the Strait of Gibraltar in the top 160 m, whereas the MOW outflow occurs below 160 m depth [*Bryden and Kinder*, 1991]. Inflowing AWs are a mix of NACW, North Atlantic Surface Waters, and shelf-influenced waters from the Gulf of Cadiz Water (GCW [*Elbaz-Poulichet et al.*, 2001a]), while MOW consists mainly of modified Levantine Intermediate Water (LIW; *Millot* [1999]).

3.2. Mediterranean Sea

Based on its stratification, the water column of the MS can be defined as a three-layer system [*Ribera d'Alcalà et al.*, 2003], with a surface (0–200 m), an intermediate (200–600 m), and a deep (600 m to bottom) layer. The general hydrography of the section has been described in great detail in *Millot and Taupier-Letage* [2005a, 2005b] and in *Rolison et al.* [2015]. Here we describe briefly some of the key features.

The surface circulation of the MS is mainly driven by incursion of the AWs that follow the continental slopes in a counterclockwise circulation (Figure 2b). Along their transport, AWs are modified by the strong evaporation in the Eastern Mediterranean Basin, leading to the warmest and saltiest surface waters observed close to Rhodes Island (Figure 2b). AWs are also modified by mixing with the low-density Black Sea waters in the North Aegean Sea and with the freshwaters of the Pô River in the Adriatic. The surface Mediterranean Sea is highly stratified from spring to late fall, and the residence time of surface waters is short on the time scale of decades [*MerMex group*, 2011]. Thus, hydrographic exchanges between surface and deeper waters are limited, and they predominantly occur where intermediate and deep waters are formed or with upwelling cells that mix intermediate waters with the surface AW [*Millot*, 1987] in the Western Basin. Both the northeastern and northwestern parts of the MS are subject to intense dry and cold Northern winds during winter, generating cold dense waters prone to deep convection. Wind stress is especially intense in the north Levantine Basin, southeast of Rhodes Island. There, the AWs are the warmest and the saltiest (Figure 2b). Winter cooling in this area leads to convection of a large volume of water to the intermediate and deep waters (up to 2000 m) which form the LIW and then spread in the whole basin at ~200–600 m (Figure 2a). Similarly to AW circulation, LIWs are transported by Coriolis force and mixed with deep waters by mesoscale instabilities along the entire Mediterranean Sea. Due to the topography, LIWs only penetrate into the Western Basin across the Sicily Channel (Figure 2a). In the Western Basin, modified LIWs follow the northern continental slopes and finally flow out of the Gibraltar Strait (Figure 2a). Additionally to LIW, specific intermediate waters are also formed in the Cretan Sea, Adriatic Sea, the Gulf of Lion, and the Ligurian Sea [*Millot*, 1999].

The Eastern Mediterranean Deep Waters (EMDWs) are formed in two distinct areas (Figure 2a): in the Cretan Sea where the LIWs mix with the dense Aegean Deep Waters and in the North Ionian Sea where the modified LIWs mix with the Adriatic Deep Waters. Due to their high density, these two similar dense water masses dive to form EMDWs, which circulate counterclockwise along the slopes below 600 m depth. In the Western Basin, the Western Mediterranean Deep Waters are formed in the Gulf of Lion. Denser WMDWs are trapped in the deep (>2000 m) western side of the basin. At shallower depths, (600–2000 m) modified WMDWs can enter into the Tyrrhenian Sea where they mix with LIW and EMDW to form the Tyrrhenian Deep Waters (TDW). The Bernoulli effect at Gibraltar Strait [*Kinder and Parrilla*, 1987] is responsible for the more intense circulation and the shorter residence time of deep waters in the Western Basin (~25 years) [*Bethoux*, 1980] compared with the residence time in the Eastern Basin (~140 years) [*van Cappellen et al.*, 2014]. The Mediterranean circulation is summarized in a simplistic hydrologic six-box model that is used in this study (Figure 2c).

4. Results and Discussion

4.1. Biogeochemistry of Cobalt in the Eastern Atlantic and in the Alboran Sea

4.1.1. Atlantic Sector (Stations 1a to 4a)

In the Eastern temperate Atlantic (stations 1a to 3a), DCo concentrations ranged between 14.4 and 83.5 pM. DCo was mostly composed of sCo, and the vertical profiles showed a typical hybrid distribution (Figures 3 and 4a). A nutrient-type behavior could be distinguished with low surface concentrations (0–200 m) of DCo (DCo < 30 pM) increasing with depth. A significant correlation between DCo and phosphates (PO_4^{3-}) was observed within the top 200 m with a DCo-PO_4^{3-} slope of 77 μM/M ($n = 18$, $R^2 > 0.9$). Concentrations of pCo in the surface (>2 pM) were slightly higher than those in the deep waters. The depth of the pCo maximum coincided with the depth of the Chlorophyll *a* maximum (Chl *a* max; Figure 3), while the maxima in DCo concentrations occur at the maximum in apparent oxygen utilization (AOU). All these features together suggest biological uptake of DCo by the phytoplankton community followed by remineralization of dead sinking phytoplankton cells by heterotrophic bacteria at depth releasing DCo at intermediate depth. DCo maxima between 750 and 1000 m depth are likely linked to the strong increase of sCo (station 3a; Figure 3), indicating that degradation of biogenic particulate matter mainly releases dissolved cobalt as sCo. Just below these maxima, sCo decreased quickly while cCo stayed relatively high (station 3a; Figure 3), suggesting

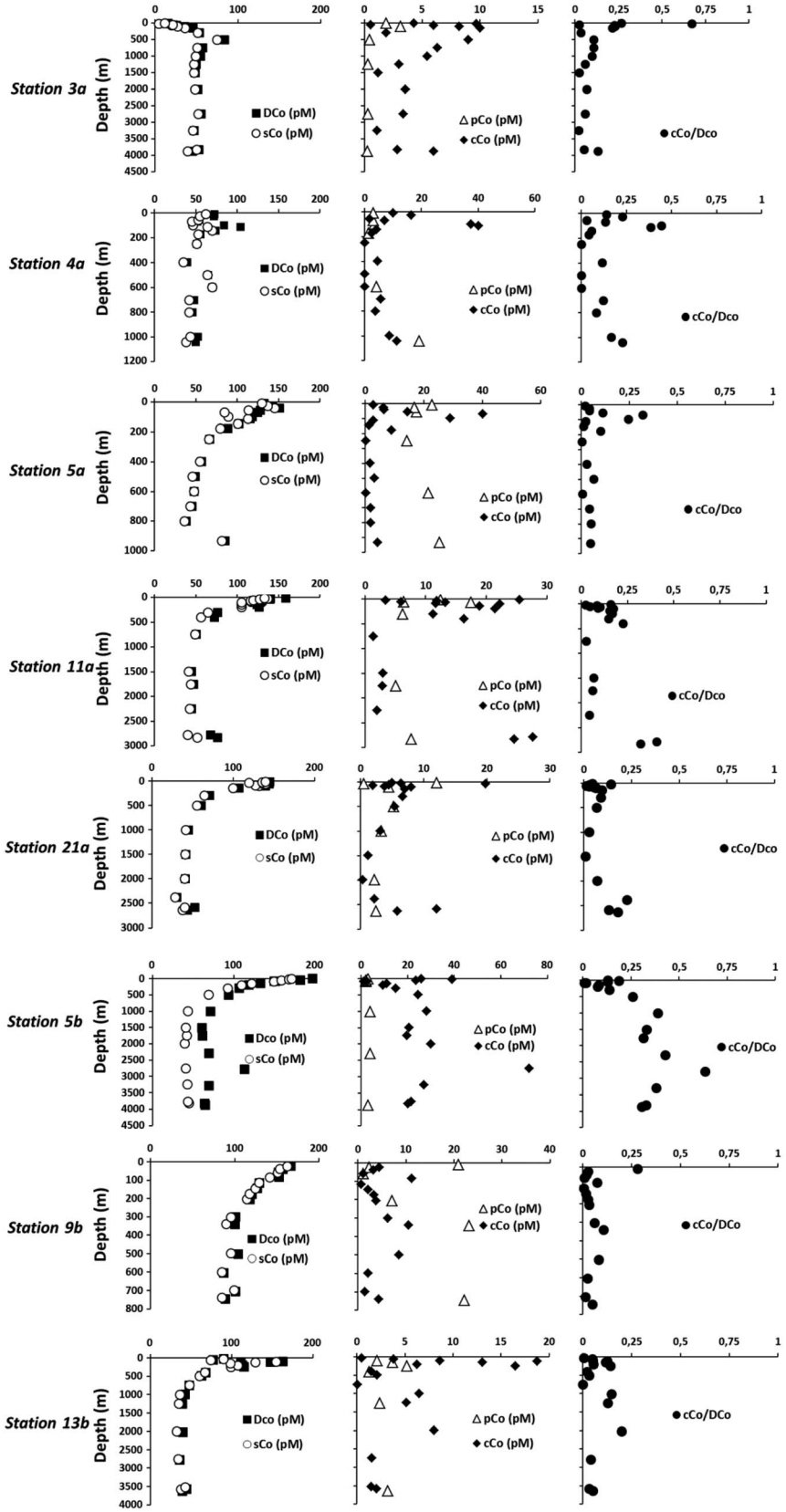

Figure 3. Vertical distributions of dissolved (DCo, black squares), soluble (sCo, open dots), colloidal (cCo, black diamonds), and particulate (triangles) cobalt and of cCo/DCo ratio (dark dots) at selected stations.

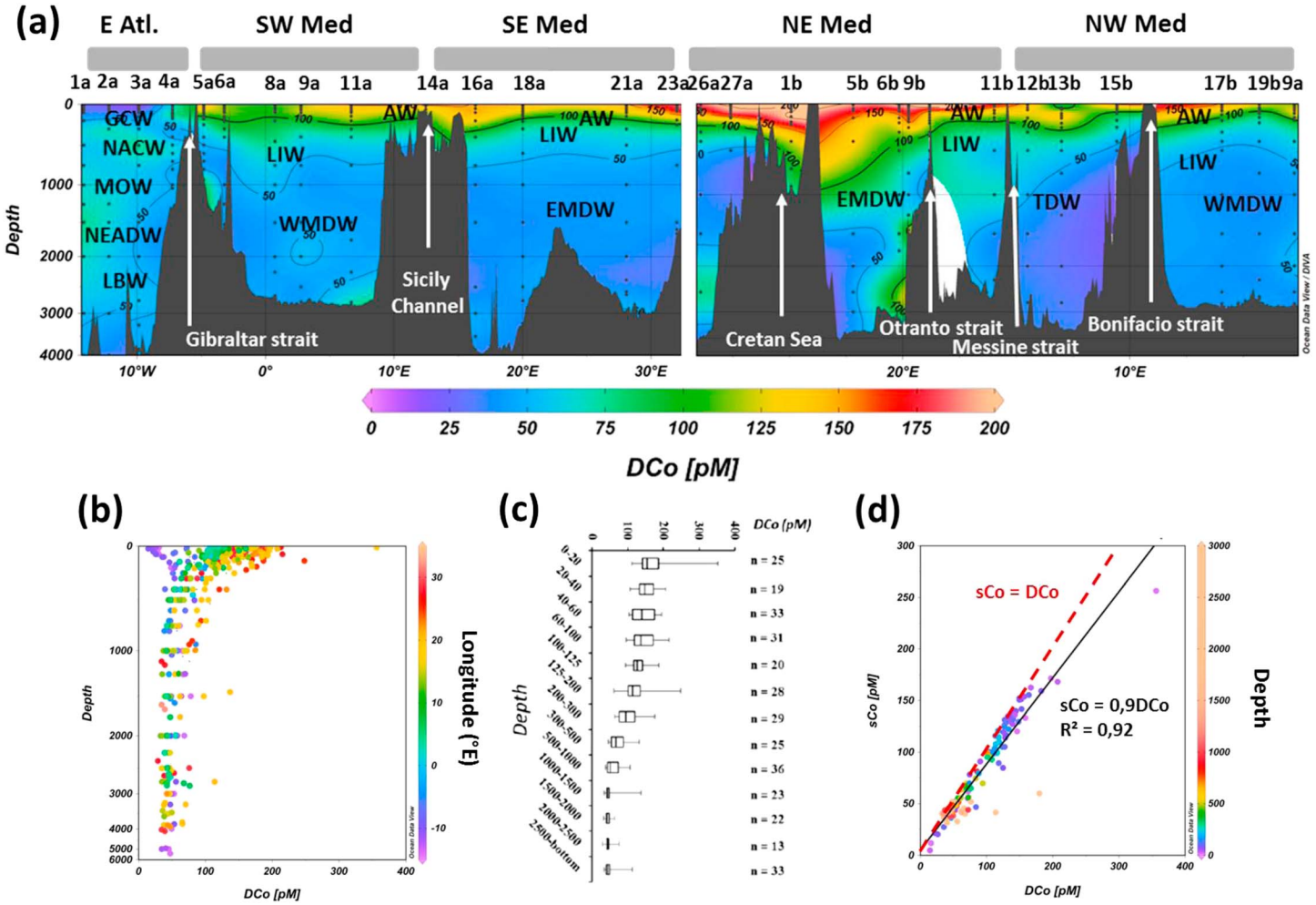

Figure 4. (a) Spatial and vertical distributions of dissolved cobalt (DCo) along the (left) southern and (right) northern routes of the section referred in Figure 1. Sampling stations and water masses are labeled. Figure created by using Ocean Data View. (b) Scatter plot of all DCo measurements performed along the GA04N section; *z* axis indicates the longitude. (c) Box whisker plots of DCo versus depth in the Mediterranean Sea. (d) Soluble (sCo) versus DCo cobalt concentrations measured along the section.

precipitation of sCo into small colloids. Nevertheless, cCo concentrations were extremely low below 1200 m depth and sCo precipitation may have been restricted only to the lower edge of the low-oxygenated layer. In the MOW, a DCo signature of ~55 pM solely occurring as sCo was recorded (Figures 3 and 4a). DCo increased westward in the MOW (Figure 4), as a result of mixing with the DCo-rich NACW. Below 1500 m, relatively high DCo concentrations recorded in the core of the young NEADW (Figure 4a) were likely due to the influence of the LSW [*van Aken*, 2000a], a water mass enriched in DCo [*Dulaquais et al.*, 2014a]. Finally, DCo concentrations decreased slowly between 2000 m and the seafloor, likely resulting from the spreading of LDW influenced by AABW [*van Aken*, 2000a], a water-mass depleted in DCo [*Dulaquais et al.*, 2014a]. Close to the bottom, both cCo and pCo increased and sCo decreased (Figure 3), suggesting sediment resuspension and net sCo adsorption/precipitation in this area.

On the West side of Gibraltar Strait (station 4a; Figure 3), the top 25 m were characterized by high DCo concentrations (~70 pM) associated with relatively high particulate aluminum and iron concentrations (pAl = 8.9 nM, pFe = 2.3 nM). These relatively high concentrations likely reflect the lithogenic influence of the Spanish shelf as dust input tends to be low in this area [*Guieu et al.*, 2010]. In the Chl *a* max (60 m depth), DCo dropped to 53 pM. While cCo stayed constant (7–10 pM), sCo strongly decreased, and both pCo and particulate phosphorus (pP) concentrations increased (pCo = 3.4 pM; pP = 46.8 nM), indicating that sCo may be utilized by the phytoplankton community. Deeper, at 115 m, the Gulf of Cadiz Waters (GCWs; salinity of

36.4 and a temperature of 16°C [*Morley et al.*, 1997]) contained high concentrations of DCo (>100 pM) as previously reported for other trace elements [*Boyle et al.*, 1985; *Van Geen et al.*, 1991; *Elbaz-Poulichet et al.*, 2001a]. Interestingly, cCo accounted for half of these high DCo concentrations (Figure 3), suggesting an intense release of cCo from the shelf system in the Gulf of Cadiz. Deeper, typical DCo concentrations were recorded in the different water masses, with a concentration of ~70 pM in the NACW (Figure 4a) and low concentrations at the bottom in the MOW outflow (~45–50 pM). Again, close to the bottom depth, cCo and PCo increased, whereas sCo decreased, which we attribute to sediment resuspension (Figure 3).

4.1.2. Alboran Sea (Stations 5a and 6a)

On the eastern side of the Gibraltar Strait (station 5a), subsurface DCo (10 m depth) concentrations were very high (>130 pM) compared to concentrations in the surface waters of the Eastern Atlantic (Figures 3 and 4a). Here high subsurface concentrations in particulate aluminum, iron, manganese, lead, and chromium (pAl = 236 nM, pFe = 56 nM, pMn = 1.7 nM, pPb = 20 pM, and pCr = 171 pM) suggest the input of lithogenic- and anthropogenic-influenced particles. Since this area also receives a low input of Saharan dust [*Guieu et al.*, 2010], these subsurface-enhanced DCo concentrations can be attributed to a strong riverine and shelf enrichment of the penetrating AWs during their transport in the Gulf of Cadiz, as previously shown for other trace metals [*van Geen et al.*, 1988]. Moreover, the mining activities in the Iberian Pyrite Belt are known to increase the trace element concentrations of southern Spanish rivers [*Braungardt et al.*, 2003] which enhance trace metal concentrations in the penetrating AW [*Elbaz-Poulichet et al.*, 2001a]; thus, the DCo enrichment of AW is probably forced by anthropogenic activities.

Interestingly, in the Eastern Alboran Sea (station 6a, Figure 4a), surface DCo was significantly lower in the upper 100 m (~117 pM) compared with station 5a closer to the Gibraltar Strait. The eastward decrease of surface DCo could be related, among other processes, to biological uptake of sCo and subsequent export of the biogenic material during the transport of the AW. Indeed, these waters were characterized by a high biomass [*van de Poll et al.*, 2015], a strong decrease in sCo concentrations toward the deep Chl *a* max (sCo = 84.1 pM), and high pCo and pP concentrations (Figure 3; PCo > 17 pM, pP > 40 nM), indicating high biological uptake of sCo in this area (Table 2). Intermediate (200–600 m) and deep (600–1000 m) waters of the Alboran Sea showed similar DCo concentrations as those found in other areas of the MS (Table 1), and DCo strongly decreased with depth (Figures 3 and 4a). Here the westward advection of low DCo in deep waters and the eastward transport of DCo rich surface waters (Figure 4a) create a strong vertical gradient of DCo concentration, resulting in an apparent scavenged-like DCo distribution. A similar process was also observed in the Western Atlantic [*Dulaquais et al.*, 2014a]. Close to the seafloor, strong DCo enrichment (mostly as sCo) coincided with high pCo concentrations at station 5a (Figure 3) and, to a lesser extent, at station 6a, indicating sedimentary inputs of sCo and pCo in this area.

4.1.3. DCo Fluxes at Gibraltar Strait

From the Atlantic to the Alboran Sea, the eastward surface DCo concentrations strongly increase (Figures 3a–3c, and 4a), showing that the advection of AW enriched in DCo is an important source of Co to the MS. In order to quantify these inputs, we have estimated the DCo fluxes across the Gibraltar Strait. The entrance of the strait could not be sampled during the cruise; therefore, we assumed that surface DCo concentrations at station 5a (0–100 m, S < 37.4, DCo = 133.0 ± 12.2 pM, $n = 6$) are representative for the inflowing AW at the strait. The salinity balance between station 3a and station 5a was checked in order to ensure that the rest of the MS is not affecting surface DCo concentrations at station 5a. Using the mean surface water inflow of 0.81 Sv determined by *Soto-Navarro et al.* [2010], we estimated an input of $9.3 \pm 0.9 \cdot 10^3$ mol DCo d^{-1} to the MS. The outflow flux of DCo was estimated at $4.5 \pm 1.4 \cdot 10^3$ mol DCo d^{-1}, using the mean DCo concentration recorded in the LIW of the Alboran Sea (mean $DCo_{200-600m} = 68.2 \pm 20.7$ pM) and a mean outflowing water flux of 0.76 Sv [*Soto-Navarro et al.*, 2010]. Similar to other studies [*Elbaz-Poulichet et al.*, 2001b; *Gómez*, 2003], these estimations suggested that Gibraltar Strait acted as a net source of DCo (~$4.8 \pm 1.5 \cdot 10^3$ mol DCo d^{-1}) for the MS. Our estimation is 20% higher than the estimation of *Gómez* [2003] which could be expected since DCo was analyzed after UV digestion of the samples in our study, unlike in the other studies.

4.2. Biogeochemistry of Co in the Mediterranean Sea

In the entire MS, the distribution of DCo showed high surface concentrations (DCo > 100 pM and up to 353 pM) decreasing with depth to a quasi-constant concentration (~45 pM) in deep waters (Table 1 and Figures 4b and 4c), resulting in a scavenged-type profile (Figure 4). Size partitioning shows that DCo

Table 1. Averaged Concentrations and Standard Deviations of Dissolved (DCo), Soluble (sCo), Colloidal (cCo), and Particulate (pCo) Cobalt in the Different Sub-Basins of the Mediterranean Sea[a]

Basin	West			East			
Sub-Basin	Alboran Sea	Central	Tyrrhenian Sea	Ionian Sea	Levantine	Cretan	Aegean
			Surface (0–200 m)				
DCo (pM)	118.3 *n* = 18 (88.3–151.4)	120.2 ± 20.9 *n* = 40 (61.3–174.9)	121.4 ± 24.6 *n* = 17 (76.3–163.9)	154.9 ± 40.8 *n* = 8 (104–353.3)	153.6 ± 22.9 *n* = 19 (107.1–184.8)	186.6 ± 27.1 *n* = 18 (118.7–248.1)	175.2 ± 12.3 *n* = 8 (149.6–192.5)
sCo (pM)	106.3 ± 21.1 *n* = 8 (79.4–136.6)	119.1 ± 11.8 *n* = 8 (105.1–136.9)	113.6 ± 24.3 *n* = 6 (90.9–152.2)	144.0 ± 31.0 *n* = 21 (103.3–326.4)	129.6 ± 14.8 *n* = 6 (100.3–139.8)	ND	ND
cCo (pM)	7.8 ± 5.0 *n* = 8 (2.8–14.4)	14.4 ± 8.2 *n* = 8 (3.4–25.5)	10.5 ± 7.0 *n* = 6 (0–18.7)	9.3 ± 11.3 *n* = 21 (0–39.1)	5.6 ± 2.4 *n* = 6 (1.9–8.0)	ND	ND
pCo (pM)	11.9 ± 8.3 *n* = 6 (2.7–22.9)	24.4 ± 50.6 *n* = 8 (1.2–158.5)	3.7 ± 1.5 *n* = 4 (2.1–5.2)	4.6 ± 7.2 *n* = 7 (1.0–20.0)	5.1 ± 0.9 *n* = 2 (4.5–5.8)	12.1 ± 17.2 *n* = 4 (1.7–37.7)	10.5 ± 7.0 *n* = 6 (4.2–12.8)
			Intermediate Layer (200–600 m)				
DCo (pM)	68.2 ± 20.7 *n* = 7 (48.0–98.4)	73.2 ± 22.0 *n* = 11 (47.8–126.5)	67.4 ± 8.5 *n* = 7 (52.5–78.2)	93.2 ± 23.6 *n* = 14 (53.4–143.2)	76.7 ± 13.7 *n* = 5 (60.9–94.1)	110.6 ± 43.5 *n* = 5 (93.3–134.3)	108.1 ± 22.1 *n* = 3 (86.8–130.8)
sCo (pM)	53.8 ± 9.2 *n* = 4 (46.2–66.2)	60.5 ± 6.2 *n* = 2 (56.1–64.9)	69.6 ± 7.7 *n* = 3 (63.3–78.2)	85.9 ± 21.0 *n* = 7 (48.8–114.4)	60.1 ± 6.4 *n* = 2 (55.4–64.6)	ND	ND
cCo (pM)	1 ± 0.2 *n* = 1	13.7 ± 3.6 *n* = 2 (11.2–16.3)	0.5 ± 0.8 *n* = 3 (0–1.5)	10.4 ± 8.0 *n* = 7 (3.8–24.5)	6.1 ± 0.9 *n* = 2 (5.5–6.7)	ND	ND
pCo (pM)	13.3 ± 1.5 *n* = 2 (12.2–14.3)	4.3 ± 2.9 *n* = 2 (2.2–6.2)	1.3 ± 0.1 *n* = 1	5.25 ± 0.5 *n* = 1	2.3 ± 0.2 *n* = 4 (2.0–2.4)	11.4 ± 2.0 *n* = 2 (10.0–12.8)	18.0 ± 3.3 *n* = 2 (15.7–20.3)
			Deep Layer (600 m to Bottom Depth)				
DCo(pM)	53.8 ± 15.7 *n* = 7 (38.4–85.6)	47.2 ± 8 *n* = 30 (38.6–76.3)	41.9 ± 7.7 *n* = 15 (32.6–60.0)	59.2 ± 24.6 *n* = 32 (34.8–137.0)	44.6 ± 11.2 *n* = 17 (28.8–75.7)	56.2 ± 20.8 *n* = 12 (34.3–93.3)	
sCo (pM)	51.5 ± 24.1 *n* = 7 (36.5–81.4)	44.9 ± 4.5 *n* = 6 (40.0–51.7)	41.8 ± 3.7 *n* = 7 (36.5–48.5)	44.2 ± 16.5 *n* = 14 (31.3–99.6)	44.4 ± 4.2 *n* = 5 (41.2–51.3)	ND	
cCo (pM)	3.1 ± 1.6 *n* = 2 (1.9–4.2)	10.3 ± 12.3 *n* = 6 (1.4–27.7)	BLD *n* = 7	17.2 ± 18.6 *n* = 14 (1.4–72.3)	1.5 ± 0.8 *n* = 5 (0.7–2.6)	ND	ND
pCo (pM)	18.6 ± 6.1 *n* = 4 (11.4–25.3)	7.2 ± 6.1 *n* = 4 (0.8–15.3)	3.2 ± 0.3 *n* = 1	7.4 ± 8.4 *n* = 7 (1.2–22.2)	2.3 ± 0.2 *n* = 4 (2.0–2.4)	6.0 ± 0.6 *n* = 1	

[a]Numbers in brackets are ranges of concentrations. ND and BLD mean not determined and below detection limit, respectively.

mainly consisted of sCo (Figure 4d), but cCo represented a substantial fraction of DCo in the surface and bottom layers (Figures 3 and 4d). The pCo concentrations were low in open sea and followed the same distribution of that of cCo (Figure 3). Nevertheless, despite similar trends, specific features were observed in the spatial distribution of the different Co fractions across the MS.

Through the Gibraltar Strait, AWs provide a "preformed" DCo concentration of ~130 pM to the Mediterranean surface layer, then along AW pathway (Figure 2b), the surface mean DCo concentrations (0–200 m) increased eastward to up to ~200 pM in the Cretan Sea and decreased in the westward return flow of the AW to as low as ~100 pM in the central Western Basin (Figures 4 and 5a). Considering a simplistic but realistic AW circulation (Figure 2b), the variations of surface DCo concentrations along AW pathway could be explained by more intense sources (atmospheric inputs, regeneration, and margin inputs) in the southern part of the MS and more intense sinks (biological uptake and surface to deep export) in the northern part. In the intermediate layer, higher DCo concentrations were recorded in the Cretan Sea compared to those in the other sub-basins (Table 1 and Figure 4a). There, LIWs are newly formed by downwelling of DCo-rich surface waters and then

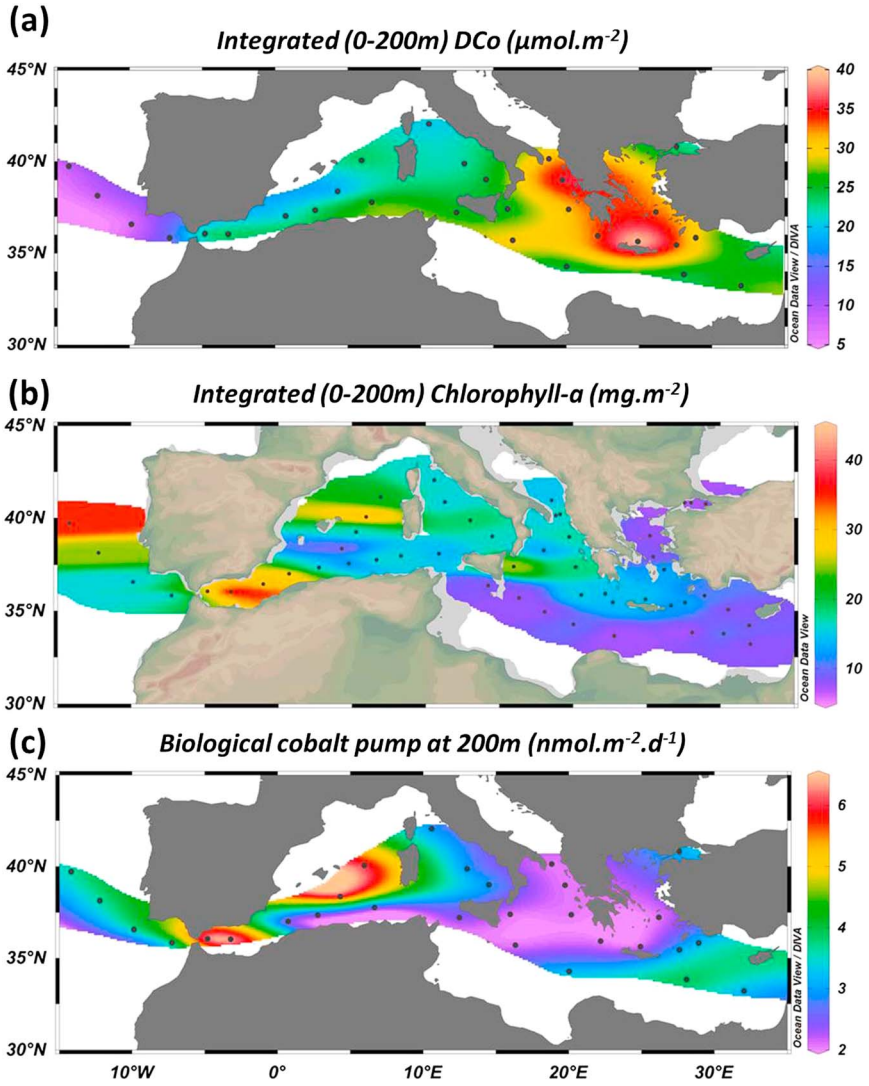

Figure 5. Spatial distribution of (a) integrated surface DCo concentration (0–200 m); (b) integrated surface chlorophyll concentrations (0–200 m, derived from fluorescence); (c) integrated cobalt biological pump at 200 m along the GA04N section. Figure created by using Ocean Data View.

spread across the different sub-basins. Deep-sea enrichment was also observed in the North Ionian Sea and, to a lesser extent, in the Cretan Sea (Figure 4a). The deep convection of intermediate waters in these areas may transport DCo to the deep sea. Finally, close to the seafloor and close to margins, high pCo and slight enrichments of DCo (Figure 3 and 4a) were measured, reaching up to 158.5 pM and 106.7 pM, respectively. In the following sections, the various processes responsible for the observed distributions are discussed.

4.2.1. Atmospheric Deposition

Atmospheric deposition is generally not considered to be important as a source of DCo to the surface open ocean [*Saito and Moffett*, 2002; *Shelley et al.*, 2012; *Dulaquais et al.*, 2014b]. However, this input can be significant in the MS since it receives extremely high dust fluxes due to its proximity with the Saharan desert [*Chester et al.*, 1977]. The atmospheric deposition rate of DCo is relatively well documented in the Western Basin of the Mediterranean Sea [*Guieu et al.*, 1997; *Migon et al.*, 1997; *Heimbürger et al.*, 2011]. Using an area of the Western Basin of $0.85 \cdot 10^{12}$ m^2, a mean atmospheric flux of total Co determined by *Migon et al.* [1997], and a partitioning coefficient given by *Guieu et al.* [1997], the total atmospheric input of DCo can be estimated to $2.2 \cdot 10^3$ mol DCo d^{-1} for the Western Basin, as described in *Heimbürger et al.* [2011]. This estimation is in accordance with the study of *Elbaz-Poulichet et al.* [2001b], who estimated a total atmospheric input of DCo ranging from 0.7 to $5.2 \cdot 10^3$ mol DCo d^{-1} based on the study of *Guieu et al.* [1997]. As far as we know,

there is unfortunately no direct measurement of the total atmospheric Co deposition in the Eastern Basin. However, the monthly and annual atmospheric depositions are well documented for other trace metals, especially aluminum, a tracer of the Saharan dust for which the deposition rate was estimated at 2.3 ± 1.5 mg Al m^{-2} d^{-1} [*Guieu et al.*, 2010]. The composition of Eastern Mediterranean aerosols has been described by *Güllü et al.* [2000], showing a stable Co:Al ratio of ~$5 \cdot 10^{-4}$ g g^{-1} in summer and winter Eastern Mediterranean aerosols. With these estimations and the partitioning coefficient of Co in Mediterranean aerosols (10%) given by *Guieu et al.* [1997], we estimated a total atmospheric input of $3.2 \pm 2.1 \cdot 10^3$ mol DCo d^{-1} for the Eastern Mediterranean Basin (an area of $1.65 \cdot 10^{12}$ m^2). Despite uncertainties, these calculations provide an estimate of the total atmospheric DCo flux over the MS (~$5.4 \cdot 10^3$ mol DCo d^{-1}), which is nearly 2 times lower than DCo surface input at Gibraltar Strait (~$9.3 \cdot 10^3$ mol DCo d^{-1}).

Atmospheric deposition probably accounts for the eastward increase of DCo concentrations along the AW pathway (Figures 4b and 5a), and the vertical distribution of cCo which generally showed enrichment in the upper 25 m (Figure 3) suggests that the atmosphere could be a source of colloidal Co in the surface layer. Moreover, the deposition of dust may have also impacted pCo and other particulate trace elements, as suggested by subsurface enrichment (Figures 3 and 7). The strong correlations recorded between pCo and pAl or pMn in the mixed layer (pCo/pAl = $0.2 \cdot 10^{-3}$ M/M, $R^2 > 0.9$; pCo/pMn = $45 \cdot 10^{-3}$ M/M, $R^2 > 0.9$) gave slopes in the range of the Co:Mn and Co:Al ratios measured in Mediterranean aerosols [*Guieu et al.*, 1997; *Güllü et al.*, 2000; *Heimbürger et al.*, 2010], strongly supporting a lithogenic origin of pCo in the mixed layer. Nevertheless, the atmospheric deposition of trace elements is known to vary geographically and temporally in the MS [*Guieu et al.*, 2010]; thus, an accurate estimation of this flux is difficult to process. The regional sea-surface atmospheric deposition of Co and other trace elements in the Mediterranean Sea will be estimated by using a new model based on surface pAl data set and discussed in details elsewhere [*Dulaquais et al.*, in prep.].

4.2.2. Biological Uptake

Biological uptake is known to be a sink of DCo in oligotrophic waters and an internal source of pCo [*Noble et al.*, 2008; *Bown et al.*, 2011; *Dulaquais et al.*, 2014b; *Twining et al.*, 2015]. In the upper 200 m where Chlorophyll *a* was higher than 0.1 mg m^{-3} (called productive layer hereafter), the pP and pCo to pAl and to particulate titanium (pTi) ratios (see Figure S1 in the supporting information) were clearly higher (0.5 M/M < pP/pAl < 38.4 M/M; 0.2 mM/M < pCo/pAl < 9.1 mM/M) than those found in the upper continental crust (pP/pAl = 0.02 M/M; pCo/pAl = 0.1 mM/M) [*Rudnick and Gao*, 2003]. Knowing that pAl and pTi are driven by lithogenic inputs [*Dammshäuser et al.*, 2013], these results suggest that both P and Co were mainly associated with the biogenic fraction. We estimated the biogenic pCo ($pCo_{biogenic}$) and pP ($pP_{biogenic}$) following equation (2).

$$pX_{biogenic} = pX - (X/Al_{aerosols} * pAl) \quad (2)$$

where pX is the particulate concentration of X, $X/Al_{aerosols}$ is the elemental ratio between X and Al in Mediterranean aerosols (after *Güllü et al.* [2000], *Guieu et al.* [2010], and *Heimbürger et al.* [2010]), and pAl is the particulate aluminum concentration measured in this study.

The POC/PON/$pP_{biogenic}$ ratios (called hereafter C/N/P) measured in suspended particles (Table 2) were similar to those reported by *Pujo-Pay et al.* [2011] in the two Mediterranean basins, and they also fitted with the elemental composition of phytoplankton and bacteria [*Sañudo-Wilhelmy et al.*, 2001; *Ho et al.*, 2003; *Bertilsson et al.*, 2003; *Twining and Baines*, 2013] reported for the main species that dominated along the section (Table 2 [*van de Poll et al.*, 2015]). Hence, the biogenic pCo to C/N/P ratios measured in the suspended particles of the productive layer could be used to determine the Co/C/N/P biological stoichiometry and to estimate the biological demand for Co in the different sub-basins of the MS.

Along the section, the respective mean particulate ratios of Co to phosphorus (Co/P) and Co to organic carbon (Co/C) were 228 ± 159 μmol mol^{-1} ($n = 35$) and 2.0 ± 1.3 μmol mol^{-1} ($n = 20$) in the productive layer, with values ranging between 12 and 644 μmol mol^{-1} and between 0.2 and 6.1 μmol mol^{-1}. The high biodiversity in the different sub-basins of the MS [*Ignatiades et al.*, 2009] likely accounted for the wide range of ratios we reported. Although in the same order of magnitude, these ratios were slightly higher than the elemental composition of phytoplankton reported in culture experiments (Co/P = 190 ± 32 μmol mol^{-1}; Co/C = 1.5 ± 0.5 μmol.mol^{-1} [*Ho et al.*, 2003]) and in the higher range of reported values for natural phytoplankton and bacteria [*Tovar-Sánchez et al.*, 2006; *Ho et al.*, 2007; *Twining et al.*, 2011, 2015; *Twining and*

Table 2. Mean Carbon, Nitrogen, Phosphorus, and Cobalt Stoichiometry in the Surface (0–200 m) Biogenic Particles, Biological Co-Uptake Fluxes (FsCo Uptake), Biogenic Co-Export Fluxes on Settling Particles Estimated in the Different Sub-Basins of the Mediterranean Sea (See Text for the Explanation of Other Terms)

Sector	Sub-Basin	Mean C/N/P	Mean Co/P (μmol/mol)	Mean Co/C (μmol/mol)	Mean[g] PPR(mmolC^2/d)	FsCo Uptake (nmol/m^2/d)	CPE[h] (%)	Biogenic Co-Export (nmol/m^2/d)
West	Alboran Sea	82/14/1 ($n=3$	223.8 ($n=6$)	2.5	45.5[b,d]	113	4.8[d]	5.5
	Central	143/21/1 ($n=6$)	176.6 ($n=6$)	1.2	43.1[a,b]	51.7	8.7[a,f]	4.5
	Tyrrhenian Sea	121/19/1 ($n=2$)	158.3 ($n=3$)	1.2	31.2[b]	37.4	8.0[e]	3.0
East	Ionian Sea	138/21/1 ($n=3$)	249.2 ($n=3$)	1.7	26.4[a,b,c]	44.9	3.9[a]	1.8
	Levantine Basin	128/15/1 ($n=3$)	494.7 ($n=3$)	3.3	21.2[a,b,c]	70.0	4.2[a]	2.9
	Aegean Sea	ND	468.2 ($n=2$)	ND[i]	31.8[b]	104.9***	2.9[e]	3.0

[a]*Moutin and Raimbault* [2002].
[b]*Bosc et al.* [2004].
[c]*van de Poll et al.* [2015].
[d]*Sanchez-Vidal et al.* [2005].
[e]*Speicher et al.* [2006].
[f]*Miquel et al.* [2011].
[g]Local primary production rate estimated after *Moutin and Raimbault* [2002], *Bosc et al.* [2004], *van de Poll et al.* [2015], and *Sanchez-Vidal et al.* [2005].
[h]Carbon pump efficiency estimated after [a]*Moutin and Raimbault* [2002], *Sanchez-Vidal et al.* [2005], *Speicher et al.* [2006], and *Miquel et al.* [2011].
[i]ND means not determined.
***Estimated by assuming a similar Co/C ratio in the Aegean Sea and in the Levantine Basin.

Baines, 2013]. The Co/P and Co/C ratios measured vary geographically between the different sub-basins of the MS, with higher ratios in the Eastern Mediterranean than in the Alboran Sea or the Central and in the Northwestern Mediterranean basins (Table 2). Interestingly, Co/P and Co/C ratios increased eastward and reach extremely high values in the south Aegean Sea (Co/P ~468 μM/M; Table 2). This increase is possibly due to cyanobacteria which contribution to the biomass also reached its maximum in the north Levantine Basin [*van de Poll et al.*, 2015]. Indeed, these species are known to have an absolute requirement for Co to grow which cannot be compensated by another metal [*Sunda and Huntsman*, 1995; *Saito et al.*, 2002], and the extremely high Co/P (and Co/C) ratios recorded in the most Eastern Basin likely reflect the high utilization of Co by these species. Interestingly, this extremely high-surface Co/P value is similar to DCo/PO_4 ratio (560 μM/M) recorded in central Atlantic, which has been considered high for a long time compared with the other ratios recorded elsewhere [*Noble et al.*, 2008; *Bown et al.*, 2011; *Dulaquais et al.*, 2014b] but which can be now explained by the occurrence of cyanobacteria. In addition, the eastward decrease of diatoms [*van de Poll et al.*, 2015], which have a low cellular Co quota [*Ho et al.*, 2003; *Twining et al.*, 2011, 2015], might also contribute to the eastward increase of Co/P and Co/C ratios. These extremely high Co/P ratios were possibly also caused by nanomolar concentrations of PO_4^{3-} and extremely high DCo (>200 pM) in the surface waters that may have promoted the biological uptake of DCo over PO_4^{3-} and therefore increased the cellular Co/P quotas [*Ji and Sherrell*, 2008] and promoted the development of cyanobacteria [*Ahlgren et al.*, 2014].

The surface dissolved pool of Co mainly consisted in sCo (Figure 3) and the decrease of bioavailable Co form. Assuming that the Co/C ratios measured in suspended particles of the productive layer represent the cellular Co/C uptake ratios, the biological uptake rate of sCo ($FsCo_{uptake}$) can be determined by combining these ratios to the local primary production rate (PPR) published in the literature for the different sub-basins of the MS. The highest sCo uptake flux was estimated for the Alboran Sea (Table 2), reaching 113 nmol m^{-2} d^{-1}, which is consistent with the high productivity of this area and with the high abundance of *Prochlorococcus* and *Synechococcus* [*van de Poll et al.*, 2015]. In the Levantine Basin, despite extremely low productivity (Figure 5b), a high sCo uptake flux of 70 nmol m^{-2} d^{-1} was associated with a high abundance of *Prochlorococcus* [*van de Poll et al.*, 2015]. Much lower uptake fluxes were estimated in the Northwestern Basin and in the Tyrrhenian Sea (52 and 37 nmol m^{-2} d^{-1}, respectively). There, the biomass was relatively high (Figure 5b), but the low particulate Co/P and Co/C ratio (Table 2) suggested a smaller contribution of cyanobacteria and a higher contribution of diatoms as previously observed in this area [*Ignatiades et al.*, 2009].

In oligotrophic areas, surface regeneration (including biological release, grazing, and cellular lysis) of biogenic pCo can lead to a significantly lower biological Co pump [*Dulaquais et al.*, 2014b]. Yet the biological Co pump can be estimated by combining local carbon pump efficiencies (CPE; Table 2) published for the

different sub-basins with $FsCo_{uptake}$; these estimations also provide a direct estimation of the biogenic pCo export rate if we consider that remineralization of biogenic pCo occurs in intermediate water [*Dulaquais et al.*, 2014a]. Low intensities of the biological Co pump and thus low biogenic Co export fluxes were estimated throughout the section ($\leq$6 nmol sCo m^{-2} d^{-1}; Table 2 and Figure 5c). The biological Co pump seems to be more intense in the Alboran Sea, the Northwestern Basin, and in the Levantine Basin than along the African coast. The biological Co pump was significantly lower than the biological uptake, suggesting an intense regeneration of biogenic Co in the surface waters, which is in agreement with the documented high-regenerated production in the MS [*Moutin and Raimbault*, 2002]. Interestingly, lower mean DCo surface concentrations (Figure 5a) were measured in areas where the biological Co pump was of high intensity (Figure 5c), suggesting a biological control of surface DCo concentrations.

4.2.3. Remineralization of Co

Sinking biogenic particles are generally prone to remineralization processes as often shown by the correlation between major nutrients (such as PO_4^{3-}) and AOU in most marine systems [*Anderson and Sarmiento*, 1994]. In the MS, remineralization and accumulation of nutrients (including P) are less efficient than in other marine systems [*Mermex group*, 2011], as a result of ultraoligotrophy, fast transit of water masses, and high load of mineral particles. Mineral particles can indeed protect organic carbon from oxidation and remineralization [*De la Rocha and Passow*, 2007]. Regarding Co, the positive correlation between DCo and AOU recorded in the intermediate Western Atlantic [*Dulaquais et al.*, 2014a] indicated that, similarly to major nutrients, biogenic pCo can also be remineralized in the intermediate waters [*Noble et al.*, 2008]. Interestingly, such a positive DCo-AOU correlation was not observed in this study, and instead, DCo was decreasing with increasing AOU (see Figure S2). The ultraoligotrophy of the MS and the short residence times of intermediate waters may account for this peculiar feature. Indeed, the low nutrient concentrations and resulting low primary production, together with a rapid regeneration of organic material in surface waters, lead to low export of biogenic pCo from the surface to intermediate waters (Table 2). In addition, pCo could be less efficiently remineralized than pP [*Dulaquais et al.*, 2014a; *Twining et al.*, 2014; *Ohnemus et al.*, 2016] and the increase with depth of the pCo/pP ratio we measured (see Figure S2) possibly indicates a differential remineralization between pCo and pP. Thereby, low export and low remineralization rate of particulate Co would both act against the development of a clear positive DCo-AOU relationship in the intermediate waters of the MS. However, the total absence of remineralization of biogenic pCo is unlikely. Considering that about 38% of the POC leaving the 200 m depth horizon is remineralized before reaching the 1000 m depth horizon in the Western Mediterranean Sea [*Miquel et al.*, 2011] and carbon is exported following a power law function with depth, and assuming there is no preferential remineralization of carbon over cobalt, the export flux of biogenic pCo (F_z $pCo_{biogenic}$) across the intermediate and deep waters can be modeled following equation (3).

$$F_z pCo_{biogenic} = F_{200m} pCo_{biogenic} * (z/200)^{-0,3} \quad (3)$$

where z is the depth and F_{200m} $pCo_{biogenic}$ is the local flux of biological Co pump (as reported in Table 2).

Under this scenario, 28% of the $pCo_{biogenic}$ exported from the 200 m horizon could be remineralized in the intermediate layer and 17% in the deep waters (600–1500 m), resulting in total input of $\sim 0.9 \cdot 10^3$ mol DCo d^{-1} and $\sim 0.5 \cdot 10^3$ mol DCo d^{-1} in the intermediate and deep waters of the Western Basin and $\sim 1.1 \cdot 10^3$ mol DCo d^{-1} and $\sim 0.7 \cdot 10^3$ mol DCo d^{-1} in the intermediate and deep waters of the Eastern Basin (Table 3; see supplementary information for detail of calculation).

4.2.4. Physical Processes

The sharp vertical DCo gradient with high concentrations in the surface layer decreasing with depth (Figures 3 and 4b and 4c) can be indicative of a vertical diffusion supply of DCo from the surface to the deep sea. In order to provide an order of magnitude of this process, we estimated the vertical diffusion of DCo by using the mean vertical DCo gradients recorded in the different sub-basins of the MS (-2.1 nmol $m^{-4} > \partial DCo/\partial z > 0$ nmol m^{-4}) and the vertical diffusivity coefficients (0.3 cm^2 $s^{-1} \geq Kz \geq 10^{-3}$ cm^2 s^{-1}) from *Wu and Haines* [1998] (see supplementary information for detail of calculation). The higher diffusive fluxes (1–5 nmol DCo m^{-2} d^{-1}) were obtained at ~25 m, corresponding to the base of the mixed layer. This flux strongly decreased across the thermocline, reaching values close to 10^{-4} nmol DCo m^{-2} d^{-1} in the deep sea. The vertical diffusive flux stayed low at the interfaces between the three layers with a mean flux of $1.3 \pm 0.7 \cdot 10^{-2}$ nmol DCo m^{-2} d^{-1} at 200 m and of $4.7 \pm 1.1 \cdot 10^{-4}$ nmol DCo m^{-2} d^{-1} at 600 m. Below 600 m depth, DCo concentrations being homogenous, the effect of vertical diffusion can be considered negligible. At the scale of the MS

Table 3. Estimation of DCo Removal Rates in the Deep Waters of the Two Mediterranean Basins (See Text for Calculations)

Basin	West	East
Deep water residence time (years)[a]	22.0	138.4
DCo removed from the deep sea (10^6 mol)[b]	18.0	85.7
Basin scale apparent daily DCo removal rate (10^3 mol.d^{-1})	2.2	1.7
Basin scale daily remineralization flux (10^3 mol.d^{-1})[c]	0.5	0.7
Basin scale total DCo removal flux (nmol.m^{-2}.d^{-1})	2.7	2.4

[a]Estimated by using the deep layer volume divided by the intermediate convection fluxes (see Figure 2c). Values are in accordance with *Bethoux* [1980] and *van Cappellen et al.* [2014].
[b]Estimated for each basin by using the mean difference between the two end-member of DCo concentrations between the intermediate and deep layer, multiplied by the volume of the deep layer.
[c]Estimated by following a power law function; see section 4.2.3.

($2.5 \cdot 10^{12}$ m^2), the estimated mean vertical diffusive fluxes were of 32.5 ± 17.5 mol DCo d^{-1} at 200 m depth and of 1.2 ± 0.3 mol DCo d^{-1} at 600 m depth. These estimations are low compared to convective fluxes (see hereafter); hence, the vertical diffusion was likely not a significant process in the Mediterranean Co cycle.

In the North Ionian Basin and in the Cretan Sea, high intermediate and deep DCo concentrations were measured (DCo > 80 pM) compared to the other domains (Figure 4a). There, EMDWs are formed by convection of intermediate waters (250–600 m) to the deep sea [*Roether and Schlitzer*, 1991; *Lascaratos et al.*, 1999]. Deep convection feeding the entire deep Eastern Basin, it also provides preformed DCo to the deep sea. Considering the mean DCo concentration in the intermediate waters of the south Adriatic (106 ± 11.3 pM; $n = 6$) and of the Cretan Sea (110.6 ± 26.8; $n = 6$), the convection fluxes of DCo ($FDCo_{convection}$) can be estimated by multiplying these concentrations to the convection rate in the North Ionian Sea and in the Cretan Sea (~0.3 Sv and ~ 0.04 Sv, respectively) [*Roether and Schlitzer*, 1991; *Zervakis et al.*, 2004; *Van Cappellen et al.*, 2014] (see supplementary information for details of calculation). We determined an $FDCo_{convection}$ of $0.4 \pm 0.1 \cdot 10^3$ mol DCo d^{-1} in the Cretan Sea and of $2.8 \pm 0.3 \cdot 10^3$ mol DCo d^{-1} in the North Ionian Sea, which result in a total input of $\sim 3.2 \pm 0.3 \cdot 10^3$ mol DCo d^{-1} for the deep Eastern Basin. Similar calculation was applied to the Western MS by using a mean DCo concentration of 70.9 ± 16.8 pM ($n = 16$) recorded in the intermediate layer of the Northwestern MS and a convection rate of ~1.1 Sv for the WMDW (Figure 2c) [*Durrieu de Madron et al.*, 2013]. In this basin, the deep convection could provide $\sim 6.7 \pm 1.6 \cdot 10^3$ mol DCo d^{-1} to the deep sea.

In order to close the water budgets, upwelling of deep waters to intermediate depths needs to be considered to compensate deep convection (Figure 2c). Mixing of upwelled DCo poor deep waters with LIW could decrease the DCo concentration of this water mass along its pathway. A simple calculation of mixing between the two DCo end-members weighted by the water flux of each water mass was used to predict the resulting DCo after mixing (see Figure S3 for details of calculation). The DCo concentrations in the LIW flowing out through the Sicily Channel ($DCo_{LIW\text{-}SC}$) and through the Gibraltar Strait ($DCo_{LIW\text{-}GS}$) were then estimated. Interestingly, our calculations provided an estimated value of 95.3 pM for $DCo_{LIW\text{-}SC}$ and of 71.4 pM for $DCo_{LIW\text{-}GS}$, which are in excellent agreement with intermediate DCo measured at these locations (respectively 93.2 pM and 68.2 pM) and indicate that the DCo decrease along the westward pathway of LIW can be explained by mixing and dilution process. The impact of water-mass mixing on the distribution of DCo in low oxygenated intermediate layer was previously observed in the Atlantic [*Noble et al.*, 2012; *Dulaquais et al.*, 2014a] and recently in the Pacific [*Hawco et al.*, 2016].

4.2.5. DCo Fluxes at the Sicily Channel

The Sicily Channel connects the Western and the Eastern basins in a two-layer system with the modified AW at the surface flowing eastward and the LIW flowing over the bottom in a westward direction. Water fluxes across this strait are about 1.14 Sv and 1.1 Sv for the surface AW and the deep LIW, respectively (Figure 2c) [*Manzella et al.*, 1988; *Astraldi et al.*, 1999]. Based on these estimations and on our DCo measurements on both sides of the Sicily Channel, 124.5 ± 5.5 pM ($n = 6$) in the eastward flowing AW and 93.2 ± 23.6 pM ($n = 14$) in the LIW leaving the Ionian Sea, the DCo input to the surface Eastern Basin was thus estimated to be $12.3 \pm 0.6 \cdot 10^3$ mol DCo d^{-1} and the output at intermediate depths to be $8.9 \pm 2.2 \cdot 10^3$ mol DCo d^{-1}. The net input of $\sim 3.4 \pm 2.3 \cdot 10^3$ mol DCo d^{-1} into the Eastern Basin through the Sicily Chanel was similar to the net input to the Western MS at the Gibraltar Strait.

4.2.6. DCo Removal in the Intermediate and Deep Sea

The adsorption of inorganic Co onto particulate MnOx and/or its oxidation into insoluble Co oxides that precipitate are major pathways of DCo removal in the deep sea [*Murray*, 1975]. These processes (called scavenging hereafter) can be catalyzed by manganese oxidative bacteria [*Lee and Tebo*, 1994; *Moffett and Ho*, 1996] and

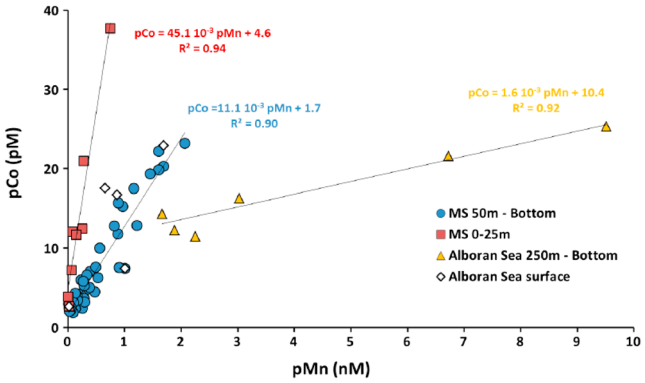

Figure 6. Particulate cobalt concentrations (pCo) versus particulate manganese concentrations (pMn) measured in the Mediterranean Sea.

lowered at low abundance of MnOx, by the complexation of DCo with soluble strong organic ligands [*Saito and Moffett*, 2001] and perhaps at low temperatures as suggested by *Saito et al.* [2010]. A strong positive correlation between pCo and pMn ($R^2 = 0.9$; $n = 43$) was recorded between 50 m and the bottom depth (Figure 6), suggesting a similar cycling of both elements in the particulate phase and possibly a removal of DCo via the MnOx pathway. However, the concentrations of both pCo and pMn were low and tend to decrease from the surface to the deep sea, with an exception at the bottom depth (Figure 7). Moreover, MnO_2 concentrations, estimated by following *Lam et al.* [2015] method ($MnO_2 = (pMn - (pTi * 0.13))$, were extremely low along the section except in the Alboran Sea (Figure 7c). These observations probably indicate that only a small fraction of DCo might be removed by MnOx pathway. A slow process of sCo precipitation in cCo is another scavenging process. Since colloids are very reactive and have very short residence times (hours to day) [*Baskaran et al.*, 1992; *Moran and Buesseler*, 1992], cCo could then sink and/or form authigenic pCo by colloid aggregation and be buried in sediments following the Brownian-pumping model [*Honeyman and Santschi*, 1989]. The similar depth distribution of cCo and pCo (Figure 3) suggests a link between these two fractions and supports the existence of a colloidal removal pathway. In this process, Co might be oxidized by manganese oxidative bacteria into Co(III), which form colloidal $Co(OH)_3$ in seawater. Then, colloidal aggregation of cobalt oxides can form authigenic pCo. Since DCo is almost entirely complexed by strong organic ligands in open ocean [*Saito and Moffett*, 2001; *Bown et al.*, 2012], the inorganic DCo available for oxidation is extremely low and probably supports a slow scavenging rate of DCo in the ocean compared with iron or Mn [*Noble et al.*, 2012]. Scavenging is an important process at the time scale of the ocean (~1000 years), but being relatively slow [*Noble et al.*, 2012], this process might be restricted in the MS due to the short residence time of the water masses in this basin (Figure 2c). Hereafter, we attempt to quantify the intensity of this process based on our measurements.

Due to remineralization of biogenic pCo in the intermediate waters, DCo concentrations should increase along the LIW pathway or at least be in excess compared with the theoretical DCo concentration in the LIW after mixing. Since such excess of DCo was not observed (see section 4.2.4), the scavenging must balance the remineralization and both fluxes should be equal in LIW (Figure S3). DCo concentrations tend to decrease with depth suggesting that DCo was removed along the deep circulation. Since the intermediate waters feed the deep MS, the DCo removed in the deep MS can be estimated by multiplying the difference of DCo concentrations at the source (in the intermediate waters in the convection areas) and in the deep waters to the volume of the deep reservoir (600 m to seafloor; Table 3). Then, the daily deep removal of DCo fluxes can be inferred by dividing this DCo amount by the residence time of the deep layer (Table 3 and Figure 2c). We estimated a removal of $\sim 1.7 \cdot 10^3$ mol DCo d^{-1} and $\sim 2.2 \cdot 10^3$ mol DCo d^{-1} for the Eastern and Western basins, respectively. It corresponds to a deep removal flux of ~1 nmol DCo m^{-2} d^{-1} for the Eastern Basin and ~2.6 nmol DCo m^{-2} d^{-1} for the Western Basin. However, the remineralization of biogenic pCo also occurs in the deep waters below 600 m (see section 4.2.3), which needs to be considered for an accurate estimation of the total scavenging flux. It results in a total scavenging flux of $2.4 \cdot 10^3$ mol DCo d^{-1} and $2.7 \cdot 10^3$ mol DCo d^{-1} in the deep Eastern and Western basins, respectively (Table 3). A simple model of these processes allows weighting the partitioning between the biogenic and authigenic fractions in the sinking particles (see Figure S3). Our model clearly shows that the pCo reaching the sediment is mainly authigenic but still contains a substantial biogenic fraction, in agreement with studies of Mediterranean sediments [*Cossa et al.*, 2014]. As shown by our 1-D model, scavenging can be an important process for the geochemistry of cobalt in the MS. At the scale of the ocean scavenging is responsible of the nonaccumulation of this micronutrient along the thermohaline circulation as evidenced by higher DCo concentration in the deep Atlantic than in the deep Pacific [*Dulaquais et al.*, 2014a; *Hawco et al.*, 2016]. Nevertheless, because this process might be slowed by low

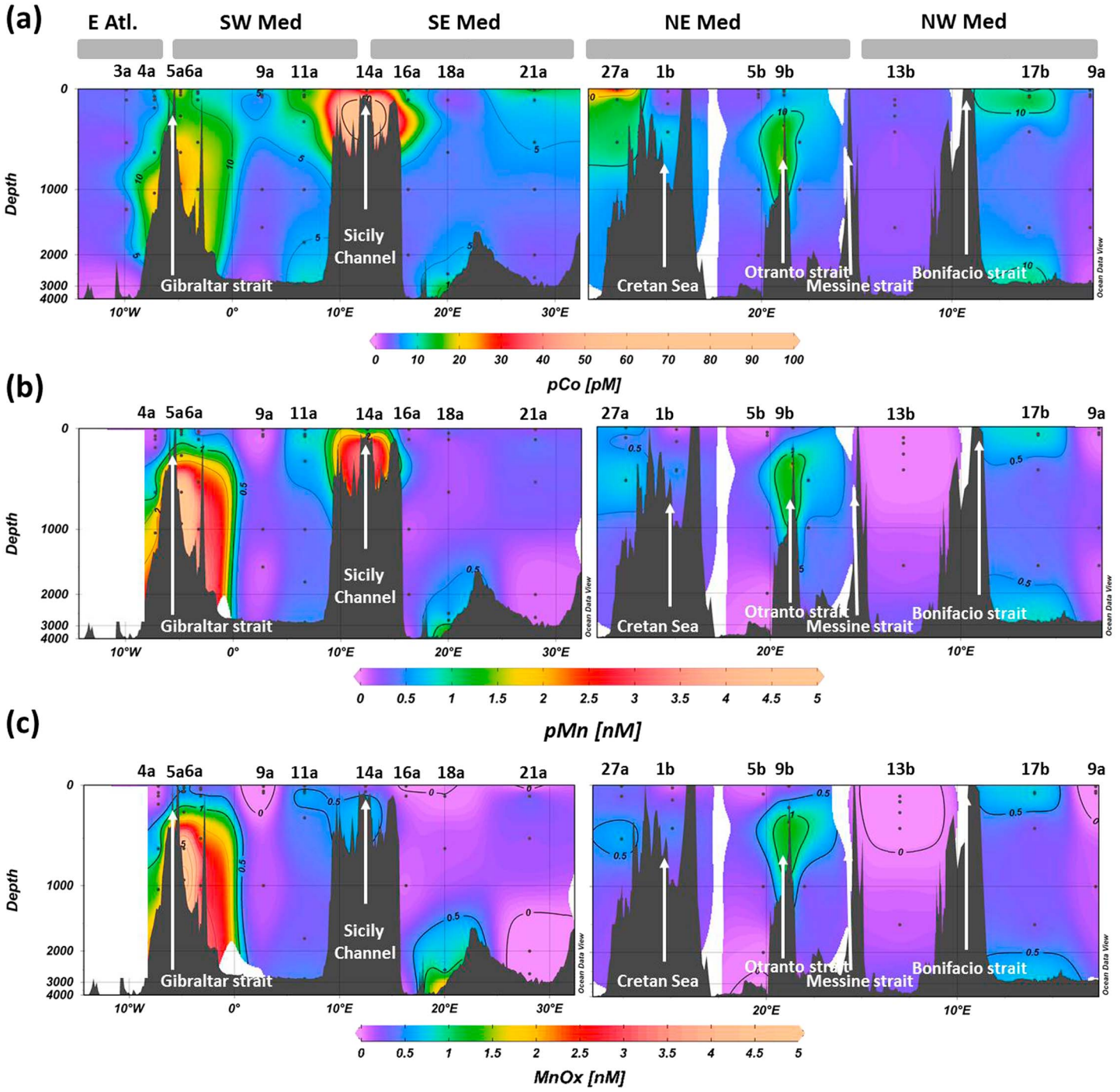

Figure 7. Spatial and vertical distributions of (a) particulate cobalt (pCo), (b) particulate manganese (pMn), and (c) particulate manganese oxides (MnOx) along the (left) southern and (right) northern routes of the section referred in Figure 1.

oxygen concentrations [*Noble et al.*, 2012] and by organic complexation [*Saito et al.*, 2001; *Bown et al.*, 2012], scavenging of DCo can be hidden by water mass mixing in area of fast circulation such as the intermediate waters of the MS and the deep West Atlantic [*Dulaquais et al.*, 2014a].

4.2.7. Benthic Input of Co

The spatial distribution of pCo and pMn in the MS (Figure 7) suggested a strong influence of the benthic and margin inputs on the particulate fraction as these concentrations increased toward the seafloor, close to margins and at straits (Figure 7). Slope currents can indeed remobilize particles from shelves and transport them

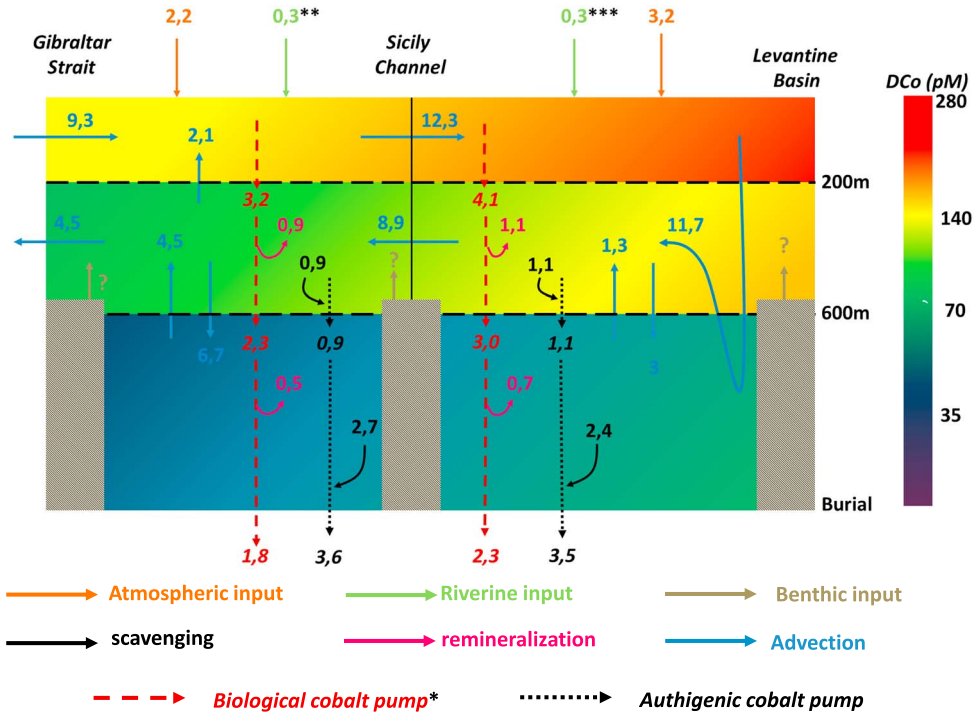

Figure 8. Conceptual diagram of dissolved cobalt biogeochemical cycle in the Mediterranean Sea. The numbers indicate fluxes in 10^3 mol DCo d^{-1}. See text for details on calculations and uncertainties. *Estimated by weighting local biological pump by the areas of the different sub-basins. **After *Elbaz-Poulichet et al.* [2001b]. ***Estimated by using mean river water discharge flux [*Struglia et al.*, 2004] and mean DCo concentrations in Pô river [*Pettine et al.*, 1994; *Tankere*, 1998] (no data available for Nile river).

toward the Mediterranean circulation. The importance of remobilization and advection of enriched particulate trace metals can be illustrated by our observations at the bottom of the Sicily Strait (Figure 7), where the highest pCo (158.5 pM), pAl (1481 nM), and pFe (439 nM) concentrations measured in the MS were observed. Local concomitant bottom relative maxima of DCo and PCo (Figures 4a and 7a) suggested a benthic source of DCo, but it is likely not linked to sediment dissolution. Indeed, Co and Mn often cycle together in the Mediterranean sediments [*Cossa et al.*, 2014], as well as in marine suspended particles (Figure 6). As the rate of Co desorption from MnOx is 3 times lower than that of adsorption in oxygenated seawater [*Murray*, 1975], Co desorption from Mediterranean sediments after resuspension is unlikely to occur in the oxygenated bottom layer ($O_2 > 180\,\mu M$). However, the reductive dissolution of MnOx in superficial sediments is known to increase the concentrations of dissolved Mn (DMn) and DCo in pore waters [*Heggie and Lewis*, 1984]. Sediment resuspension (Figure 7) and diffusion from surficial sediments could then release DCo, probably as reduced inorganic sCo (Co(II)), from pore water to the water column resulting in enrichment in sCo above the seafloor as observed in the Alboran Sea (Figure 3). Nevertheless, if the reduced sCo released from the sediment is not stabilized in solution by organic ligands, then the sedimentary input would only have a local effect: the Co (II) can be oxidized and precipitate as insoluble colloidal cobalt oxides (probably $Co(OH)_3$) and return to the sediments. The bottom cCo enrichment observed at several stations, notably at station 5b close to the Greek margin (Figure 3), could be explained by this process. The reductive dissolution and remobilization of surficial sediments could also release DMn (as Mn(II)) to the deepwater column and therefore promotes the production of MnOx by Mn (II) oxidation. These processes would enhance the adsorption rate of DCo onto MnOx surface, inducing a sink of DCo and increasing both pCo and pMn concentrations in a stoichiometric ratio. These mechanisms are proposed here to interpret the simultaneous high sCo, pCo, pMn, and MnOx concentrations measured and the strong PCo-PMn correlation (Figures 3, 6, and 7) observed in the deep waters of the Alboran Sea. Overall, further investigation on the chemical speciation of DCo in the deep MS is required to better constrain the impact of the sedimentary impact (source/sink) at basin scale.

4.3. Synoptic View of Co Biogeochemistry and Mediterranean Budget of DCo

Given the different processes we previously described and quantified, we attempted to design a synoptic view of the cobalt biogeochemistry and to establish a budget of DCo in the two Mediterranean basins (Figure 8). Briefly, the modified Atlantic Waters that penetrate at Gibraltar Strait provide a large amount of "preformed" DCo to the surface MS. Along the southern coast of the MS, this concentration increased eastward due to (i) intense Saharan deposition, (ii) eastward increase of the regeneration of biogenic pCo, and (iii) possibly to margin inputs near islands. Along the northern coast, lower Saharan inputs and the decrease of biogenic pCo regeneration induce a westward decreased of DCo in surface. The riverine inputs are significantly lower than atmospheric inputs and slightly impact the surface DCo budget (Figure 8). In the intermediate layer, remineralization of biogenic pCo is balanced by scavenging, and the decrease of DCo concentrations from the Cretan Sea to the Gibraltar Strait along the westward transit of LIW can be explained by mixing with the deep waters. Due to remineralization of biogenic material and inorganic processes of scavenging, sinking pCo was predominantly biogenic and authigenic deeper, but a substantial biogenic fraction reaches the sediments (Figure 8). In both basins, the convection of intermediate waters feeds the deep sea with relatively high DCo concentrations. However, slow but efficient scavenging, which may involve oxidation of inorganic sCo and formation of cCo and pCo by colloid aggregation, can prevent the enrichment of deep waters in DCo. The fast deep circulation of the MS can homogenize the distribution of DCo in deep waters, as exemplified by its apparent conservative behavior. Despite uncertainties, this budget is balanced in the two basins and at the scale of the Mediterranean Sea (Figure 8). This budget also highlights an important role of inputs at Gibraltar Strait on the Co cycle in the Mediterranean Sea. Together with the atmospheric input, these external sources can sustain the biological demand in the MS, in addition to provide high "preformed" DCo concentrations. This extremely high geochemical flux, which is around 2 times higher than the total atmospheric DCo inputs, is principally due to the mining activities in the Iberian Pyrite Belt [*Braungardt et al.*, 2003] that enrich the watersheds and southern Spanish rivers in trace metals [*Elbaz-Poulichet et al.*, 2001a]. However, considering the long history of this anthropogenic activity (~150 years) [*Van Geen et al.*, 1997] and the short residence time of Mediterranean waters (<150 years), the MS is probably at equilibrium with this source nowadays.

Acknowledgments

We are indebted to the captain, officers, and crew members of the R/V *Pelagia*. We would like to warmly thank Loes Gerringa and Hein de Baar for their help in organizing the cruises. We also thank NIOZ Marine Research Facilities onshore and onboard for their support. We warmly thank Jan van Ooijen, K. Bakker, E. van Weerlee, and S. Ossebaar for the analyses of nutrients, as well as S. Ober, M. Laan, S. van Heuven, S. Asjes, and L. Wuis for providing high-quality CTD data. This investigation was supported by the GEOTRACES MedBlack Seas project coordinated by M. Boye and funded by the LABEX-MER Program of the Ministère de l'Education Nationale, the L'état de l'Enseignement Supérieur et de la Recherche, and the ANR PDOC BITMAP (ANR-12-PDOC-0025-01) to H. Planquette. The Université de Bretagne Occidentale and the Région Bretagne were supporting the PhD fellowship of G. Dulaquais. Micha Rijkenberg was supported by the Netherlands Organization for Scientific Research (NWO) project grant 822.01.015 (GEOTRACES, the biogeochemical cycles of bioessential trace metals and isotopes in the Mediterranean Sea and Black Sea). This investigation is a contribution to the international GEOTRACES program. All data sets are available at the GEOTRACES data center (http://www.bodc.ac.uk).

5. Conclusions

This study presents the first comprehensive data set of cobalt in the Mediterranean Sea including both particulate and dissolved fractions. It also shows the first size fractionation data of dissolved cobalt in seawater, suggesting that DCo is mainly composed of soluble species (<20 nm) in the Mediterranean Sea.

Our works contributed to a better understanding of the multitude of processes beyond the apparent scavenged-type profile of DCo. For instance, strong geochemical inputs sustain the Co biological demand in surface. Scavenging and remineralization cannot be discerned from mixing process in the intermediate waters. In the deep sea, slow but efficient scavenging together with the short residence time of deep waters prevent the accumulation of DCo in this reservoir. Finally, the Mediterranean circulation has a strong influence on the cobalt distribution by reallocating the high-surface "preformed" DCo concentration to the entire basin and by homogenizing the DCo vertical distribution in the deep sea.

This study also highlights that inputs at Gibraltar Strait forced by human activities strongly imprint the Co distribution and may force its biogeochemistry. From our tentative budget, we show that the Mediterranean Sea seems to be now at equilibrium with this long-time Co pollution.

Nevertheless, additional works are needed for a better understanding and estimation of regional atmospheric and sedimentary fluxes that can play an important role in the Mediterranean Co cycle.

References

Ahlgren, N. A., A. Noble, A. P. Patton, K. Roache-Johnson, L. Jackson, D. Robinson, C. Mckay, L. R. Moore, M. Saito, and G. Rocap (2014), The unique trace metal and mixed layer conditions of the Costa Rica upwelling dome support a distinct and dense community of *Synechococcus*, *Limnol. Oceanogr.*, *59*(6), 2166–2184.

Anderson, L. A., and J. L. Sarmiento (1994), Redfield ratios of remineralization determined by nutrient data analysis, *Global Biogeochem. Cycles*, *8*(1), 65–80.

Astraldi, M., S. Balopoulos, J. Candela, J. Font, M. Gacic, G. P. Gasparini, B. Manca, A. Theocharis, and J. Tintoré (1999), The role of straits and channels in understanding the characteristics of Mediterranean circulation, *Prog. Oceanogr.*, *44*(1), 65–108.

Baskaran, M., P. H. Santschi, G. Benoit, and B. D. Honeyman (1992), Scavenging of thoriumisotopes by colloids in seawater of the Gulf of Mexico, *Geochim. Cosmochim. Acta*, *56*(9), 3375–3388.
Bertilsson, S., O. Berglund, D. M. Karl, and S. W. Chisholm (2003), Elemental composition of marine *Prochlorococcus* and *Synechococcus*: Implications for the ecological stoichiometry of the sea, *Limnol. Oceanogr.*, *48*, 1721–1731.
Bertrand, E. M., M. A. Saito, J. M. Rose, M. C. Lohan, A. E. Noble, P. A. Lee, and G. R. DiTullio (2007), Vitamin B_{12} and iron co-limitation of phytoplankton growth in the Ross Sea, *Limnol. Oceanogr.*, *52*, 1079–1093.
Bethoux, J. P. (1980), Mean water fluxes across sections in the Mediterranean-Sea, evaluated on the basis of water and salt budgets and of observed salinities, *Oceanol. Acta*, *3*(1), 79–88.
Bethoux, J. P., P. Morin, C. Chaumery, O. Connan, B. Gentili, and D. Ruiz-Pino (1998), Nutrients in the Mediterranean Sea, mass balance and statistical analysis of concentrations with respect to environmental change, *Mar. Chem.*, *63*(1), 155–169.
Bethoux, J. P., P. Morin, and D. P. Ruiz-Pino (2002), Temporal trends in nutrient ratios: Chemical evidence of Mediterranean ecosystem changes driven by human activity, *Deep Sea Res., Part II*, *49*(11), 2007–2016.
Bonnet, S., A. Tovar-Sanchez, C. Panzeca, E. Ortega-retuerta, C. M. Duarte, and S. A. Sanudo-Wilhelmy (2013), Geographical gradients of dissolved Vitamin B12 in the Mediterranean Sea, *Front. Microbiol.*, *4*, 126.
Bosc, E., A. Bricaud, and D. Antoine (2004), Seasonal and interannual variability in algal biomass and primary production in the Mediterranean Sea, as derived from 4 years of SeaWiFS observations, *Global Biogeochem. Cycles*, *18*, GB1005, doi:10.1029/2003GB002034.
Boutov, D., Á. Peliz, P. Miranda, P. M. Soares, R. M. Cardoso, L. Prieto, J. Ruiz, and J. García- Lafuente (2014), Inter-annual variability and long term predictability of exchanges through the Strait of Gibraltar, *Global Planet. Change*, *114*, 23–37.
Bown, J., M. Boye, A. Baker, E. Duvieilbourg, F. Lacan, F. Le Moigne, F. Planchon, S. Speich, and D. M. Nelson (2011), The biogeochemical cycle of dissolved cobalt in the Atlantic and the Southern Ocean south off the coast of South Africa, *Mar. Chem.*, *126*, 193–206, doi:10.1016/j.marchem.2011.03.008.
Bown, J., M. Boye, and D. M. Nelson (2012), New insights on the role of organic speciation in the biogeochemical cycle of dissolved cobalt in the southeastern Atlantic and the Southern Ocean, *Biogeosciences*, *9*, 2719–2736.
Boyle, E. A., S. D. Chapnick, X. X. Bai, and A. Spivack (1985), Trace metal enrichments in the Mediterranean Sea, *Earth Planet. Sci. Lett.*, *74*(4), 405–419.
Braungardt, C. B., E. P. Achterberg, F. Elbaz-Poulichet, and N. H. Morley (2003), Metal geochemistry in a mine-polluted estuarine system in Spain, *Appl. Geochem.*, *18*(11), 1757–1771.
Bryden, H. L., and T. H. Kinder (1991), Steady two-layer exchange through the Strait of Gibraltar, *Deep Sea Res. Part A*, *38*(S445), S463.
Chester, R., G. G. Baxter, A. K. A. Behairy, K. Connor, D. Cross, H. Elderfield, and R. C. Padgham (1977), Soil-sized eolian dusts from the lower troposphere of the Eastern Mediterranean Sea, *Mar. Geol.*, *24*(3), 201–217.
Cossa, D., R. Buscail, P. Puig, J. F. Chiffoleau, O. Radakovitch, G. Jeanty, and S. Heussner (2014), Origin and accumulation of trace elements in sediments of the Northwestern Mediterranean margin, *Chem. Geol.*, *380*, 61–73.
Dammshäuser, A., T. Wagener, D. Garbe-Schönberg, and P. Croot (2013), Particulate and dissolved aluminum and titanium in the upper water column of the Atlantic Ocean, *Deep Sea Res., Part I*, *73*, 127–139.
de Baar, H. J. W., et al. (2008), Titan: A new facility for ultraclean sampling of trace elements and isotopes in the deep oceans in the international GEOTRACES program, *Mar. Chem.*, *111*(1–2), 4–21.
De la Rocha, C., and U. Passow (2007), Factors influencing the sinking of POC and the efficiency of the biological carbon pump, *Deep Sea Res., Part II*, *54*(5), 639–658.
Dulaquais, G., M. Boye, M. J. A. Rijkenberg, and X. Carton (2014a), Physical and remineralization processes govern the cobalt distribution in the deep western Atlantic Ocean, *Biogeosciences*, *11*(6), 1561–1580.
Dulaquais, G., M. Boye, R. Middag, S. Owens, V. Puigcorbe, K. Buesseler, H. de Baar, and X. Carton (2014b), Contrasting biogeochemical cycles of cobalt in the surface western Atlantic Ocean, *Global Biogeochem. Cycles*, *28*, 1387–1412, doi:10.1002/2014GB004903.
Durrieu de Madron, X., et al. (2013), Interaction of dense shelf water cascading and open-sea convection in the Northwestern Mediterranean during winter 2012, *Geophys. Res. Lett.*, *40*, 1379–1385, doi:10.1002/grl.50331.
Elbaz-Poulichet, F., N. H. Morley, J. M. Beckers, and P. Nomerange (2001a), Metal fluxes through the Strait of Gibraltar: The influence of the Tinto and Odiel rivers (SW Spain), *Mar. Chem.*, *73*(3), 193–213.
Elbaz-Poulichet, F., C. Guieu, and N. H. Morley (2001b), A reassessment of trace metal budgets in the Western Mediterranean Sea, *Mar. Poll. Bull.*, *42*(8), 623–627.
Gobler, C. J., C. Norman, C. Panzeca, G. T. Taylor, and S. A. Sañudo-Wilhelmy (2007), Effect of B vitamins (B1, B12) and inorganic nutrients on algal bloom dynamics in a coastal ecosystem, *Aquatic Microbial Ecol.*, *49*(2), 181–194.
Goericke, R., and N. A. Welschmeyer (1993), The marine prochlorophyte Prochlorococcus contributes significantly to phytoplankton biomass and primary production in the Sargasso Sea, *Deep Sea Res., Part I*, *40*(11–12), 2283–2294.
Gómez, F. (2003), The role of the exchanges through the Strait of Gibraltar on the budget of elements in the Western Mediterranean Sea: Consequences of human-induced modifications, *Mar. Pollut. Bull.*, *46*(6), 685–694.
Gong, N., C. Chen, L. Xie, H. Chen, X. Lin, and R. Zhang (2005), Characterization of a thermostable alkaline phosphatase from a novel species *Thermusyunnanensis* sp. nov. and investigation of its cobalt activation at high temperature, *Biochim. Biophys. Acta*, *1750*, 103–111.
Grasshoff, K., et al. (1983), *Methods of Seawater Analysis*, pp. 419, Verlag Chemie GmbH, Weinheim.
Guieu, C., R. Chester, M. Nimmo, J. M. Martin, S. Guerzoni, E. Nicolas, J. Mateu, and S. Keyse (1997), Atmospheric input of dissolved and particulate metals to the Northwestern Mediterranean, *Deep Sea Res., Part II*, *44*(3), 655–674.
Guieu, C., M. D. Loÿe-Pilot, L. Benyahya, and A. Dufour (2010), Spatial variability of atmospheric fluxes of metals (Al, Fe, Cd, Zn and Pb) and phosphorus over the whole Mediterranean from a one-year monitoring experiment: Biogeochemical implications, *Mar. Chem.*, *120*(1), 164–178.
Güllü, G. H., İ. Ölmez, and G. Tuncel (2000), Temporal variability of atmospheric trace element concentrations over the Eastern Mediterranean Sea, *Spectrochim. Acta Part B: At. Spectrosc.*, *55*(7), 1135–1150.
Hawco, N. J., D. C. Ohnemus, J. A. Resing, B. S. Twining, and M. A. Saito (2016), A dissolved cobalt plume in the oxygen minimum zone of the eastern tropical South Pacific, *Biogeosciences*, *13*(20), 5697.
Heggie, D., and T. Lewis (1984), Cobalt in pore waters of marine sediments, *Nature*, *311*, 453–455.
Heimbürger, L. E., C. Migon, A. Dufour, J. F. Chiffoleau, and D. Cossa (2010), Trace metal concentrations in the North-western Mediterranean atmospheric aerosol between 1986 and 2008: Seasonal patterns and decadal trends, *Sci. Total Environ.*, *408*(13), 2629–2638.
Heimbürger, L. E., C. Migon, and D. Cossa (2011), Impact of atmospheric deposition of anthropogenic and natural trace metals on Northwestern Mediterranean surface waters: A box model assessment, *Environ. Pollut.*, *159*(6), 1629–1634.

Ho, T. Y., A. Quigg, Z. V. Finkel, A. J. Milligan, K. Wyman, P. G. Falkowski, and F. M. Morel (2003), The elemental composition of some marine phytoplankton, *J. Phycol.*, *39*, 1145–1159.
Ho, T. Y., L. S. Wen, C. F. You, and D. C. Lee (2007), The trace metal composition of size-fractionated plankton in the South China Sea: Biotic versus abiotic sources, *Limnol. Oceanogr.*, *52*(5), 1776–1788.
Honeyman, B. D., and P. H. Santschi (1989), A Brownian-pumping model for oceanic trace metal scavenging: Evidence from Th isotopes, *J. Mar. Res.*, *47*(4), 951–992.
Ignatiades, L., O. Gotsis-Skretas, K. Pagou, and E. Krasakopoulou (2009), Diversification of phytoplankton community structure and related parameters along a large-scale longitudinal east-west transect of the Mediterranean Sea, *J. Plankton Res.*, *31*(4), 411–428.
Ji, Y., and R. M. Sherrell (2008), Differential effects of phosphorus limitation on cellular metals in Chlorella and Microcystis, *Limnol. Oceanogr.*, *53*, 1790–1804.
Kinder, T. H., and G. Parrilla (1987), Yes, some of the Mediterranean outflow does come from great depth, *J. Geophys. Res.*, *92*, 2901–2906, doi:10.1029/JC092iC03p02901.
Lam, P. J., B. S. Twining, C. Jeandel, A. Roychoudhury, J. A. Resing, P. H. Santschi, and R. F. Anderson (2015), Methods for analyzing the concentration and speciation of major and trace elements in marine particles, *Prog. Oceanogr.*, *133*, 32–42.
Lane, T. W., and F. M. M. Morel (2000), Regulation of carbonic anhydrase expression by zinc, cobalt, and carbon dioxide in the marine diatom *Thalassiosira weissflogii*, *Plant Physiol.*, *123*, 345–352, doi:10.1104/pp.123.1.345.
Lane, T. W., M. A. Saito, G. N. George, I. J. Pickering, R. C. Prince, and F. M. Morel (2005), Biochemistry: A cadmium enzyme from a marine diatom, *Nature*, *435*(7038), 42–42.
Lascaratos, A., W. Roether, K. Nittis, and B. Klein (1999), Recent changes in deep water formation and spreading in the Eastern Mediterranean Sea: A review, *Prog. Oceanogr.*, *44*, 5–36.
Lee, Y., and B. M. Tebo (1994), Cobalt (II) oxidation by the marine manganese (II)-oxidizing *Bacillus* sp. strain SG-1, *Appl. Environ. Microbiol.*, *60*(8), 2949–2957.
Mantyla, A. W., and J. L. Reid (1983), Abyssal characteristics of the World Ocean waters, *Deep Sea Res. Part A*, *30*(8), 805–833.
Manzella, G. M., G. P. Gasparini, and M. Astraldi (1988), Water exchange between the Eastern and Western Mediterranean through the Strait of Sicily, *Deep Sea Res. Part A*, *35*(6), 1021–1035.
Mariotti, A., M. V. Struglia, N. Zeng, and K. M. Lau (2002), The hydrological cycle in the Mediterranean region and implications for the water budget of the Mediterranean Sea, *J. Clim.*, *15*(13), 1674–1690.
Martens, J. H., H. Barg, M. Warren, and D. Jahn (2002), Microbial production of vitamin B12, *Appl. Microbiol. Biotechnol.*, *58*(3), 275–285.
McCartney, M. S. (1992), Recirculating components to the deep boundary current of the northern North Atlantic, *Prog. Oceanogr.*, *29*(4), 283–383.
MerMex group (2011), Marine ecosystems' responses to climatic and anthropogenic forcings in the Mediterranean, *Progr. Oceanogr.*, *91*(2), 97–166.
Migon, C., B. Journel, and E. Nicolas (1997), Measurement of trace metal wet, dry and total atmospheric fluxes over the Ligurian Sea, *Atmos. Environ.*, *31*(6), 889–896.
Millot, C. (1987), Circulation in the Western Mediterranean-Sea, *Oceanol. Acta*, *10*(2), 143–149.
Millot, C. (1999), Circulation in the Western Mediterranean Sea, *J. Mar. Syst.*, *20*(1), 423–442.
Millot, C., and I. Taupier-Letage (2005a), Circulation in the Mediterranean Sea, in *The Handbook of Environmental Chemistry 5 (K)*, vol. 930, edited by A. Saliot, pp. 29–66, Springer, Berlin.
Millot, C., and I. Taupier-Letage (2005b), Additional evidence of LIW entrainment across the Algerian Basin by mesoscale eddies and not by a permanent westward flowing vein, *Progr. Oceanogr.*, *66*(2-4), 231–250.
Miquel, J.-C., J. Martín, B. Gasser, A. Rodriguez-y-Baena, T. Toubal, and S. W. Fowler (2011), Dynamics of particle flux and carbon export in the Northwestern Mediterranean Sea: A two decade time-series study at the DYFAMED site, *Prog. Oceanogr.*, *91*(4), 461–481.
Moffett, J. W., and J. Ho (1996), Oxidation of cobalt and manganese in seawater via a common microbially catalyzed pathway, *Geochim. Cosmochim. Acta*, *60*(18), 3415–3424.
Moran, S. B., and K. O. Buesseler (1992), Short residence time of colloids in the upper ocean estimated from 238U–234Th disequilibria, *Nature*, *359*, 221–223.
Morley, N. H., J. D. Burton, S. P. C. Tankere, and J. M. Martin (1997), Distribution and behaviour of some dissolved trace metals in the Western Mediterranean Sea, *Deep Sea Res., Part II*, *44*(3), 675–691.
Moutin, T., and P. Raimbault (2002), Primary production, carbon export and nutrients availability in western and Eastern Mediterranean Sea in early summer 1996 (MINOS cruise), *J. Mar. Syst.*, *33*, 273–288.
Murray, J. W. (1975), The interaction of cobalt with hydrous manganese dioxide, *Geochim. Cosmochim. Acta*, *39*(5), 635–647.
Ngoc, L. H., and N. E. Whitehead (1986), Nickel and cobalt determination in the North-western Mediterranean by differential pulse cathodic stripping voltammetry, *Oceanol. Acta*, *9*(4), 433–438.
Noble, A. E., M. A. Saito, K. Maiti, and C. R. Benitez-Nelson (2008), Cobalt, manganese, and iron near the Hawaiian Islands: A potential concentrating mechanism for cobalt within a cyclonic eddy and implications for the hybrid-type trace metals, *Deep Sea Res., Part II*, *55*(10), 1473–1490.
Noble, A. E., C. H. Lamborg, D. C. Ohnemus, P. J. Lam, T. J. Goepfert, C. H. Frame, K. Casciotti, G. R. DiTullio, J. Jennings, and M. A. Saito (2012), Basin-scale inputs of cobalt, iron, and manganese from the Benguela-Angola front to the South Atlantic Ocean, *Limnol. Oceanogr.*, *57*, 989–1010.
Ohnemus, D. C., S. Rauschenberg, G. A. Cutter, J. N. Fitzsimmons, R. M. Sherrell, and B. S. Twining (2016), Elevated trace metal content of prokaryotic communities associated with marine oxygen deficient zones, *Limnol. Oceanogr.*, *16*, 3–25.
Panzeca, C., A. Tovar-Sanchez, S. Agustí, I. Reche, C. M. Duarte, G. T. Taylor, and S. A. Sañudo-Wilhelmy (2006), B vitamins as regulators of phytoplankton dynamics, *Eos Trans. AGU*, *87*(52), 593–596, doi:10.1029/2006EO520001.
Panzeca, C., A. J. Beck, K. Leblanc, G. T. Taylor, D. A. Hutchins, and S. A. Sañudo-Wilhelmy (2008), Potential cobalt limitation of vitamin B12 synthesis in the North Atlantic Ocean, *Global Biogeochem. Cycles*, *22*, GB2029, doi:10.1029/2007GB003124..
Pettine, M., M. Camusso, W. Martinotti, R. Marchetti, R. Passino, and G. Queirazza (1994), Soluble and particulate metals in the Po River: Factors affecting concentrations and partitioning, *Sci. Total Environ.*, *145*(3), 243–265.
Planquette, H., and R. M. Sherrell (2012), Sampling for particulate trace element determination using water sampling bottles: Methodology and comparison to in situ pumps, *Limnol. Oceanogr. Methods*, *10*, 367–388.
Price, N. M., and F. M. M. Morel (1990), Cadmium and cobalt substitution for zinc in a marine diatom, *Nature*, *344*(6267), 658–660.
Pujo-Pay, M., P. Conan, L. Oriol, V. Cornet-Barthaux, C. Falco, J. F. Ghiglione, C. Goyet, T. Moutin, and L. Prieur (2011), Integrated survey of elemental stoichiometry (C, N, P) from the Western to Eastern Mediterranean Sea, *Biogeosciences*, *8*(4), 883–899.

Raux, E., H. L. Schubert, and M. J. Warren (2000), Biosynthesis of cobalamin (vitamin B12): A bacterial conundrum, *Cellular Molecular Life Sci. CMLS*, *57*(13-14), 1880–1893.
Ribera d'Alcalà, M., G. Civitarese, F. Conversano, and R. Lavezza (2003), Nutrient ratios and fluxes hint at overlooked processes in the Mediterranean Sea, *J. Geophys. Res.*, *108*(C9), 8106, doi:10.1029/2002JC001650.
Rijkenberg, M. J., et al. (2015), "PRISTINE", a new high volume sampler for ultraclean sampling of trace metals and isotopes, *Mar. Chem.*, *177*, 501–509.
Rodellas, V., J. Garcia-Orellana, P. Masqué, M. Feldman, and Y. Weinstein (2015), Submarine groundwater discharge as a major source of nutrients to the Mediterranean Sea, *Proc. Natl. Acad. Sci. U.S.A.*, *112*(13), 3926–3930.
Roether, W., and R. Schlitzer (1991), Eastern Mediterranean deep water renewal on the basis of chlorofluoromethane and tritium data, *Dyn. Atmos. Oceans*, *15*(3), 333–354.
Rolison, J. M., R. Middag, C. H. Stirling, M. J. A. Rijkenberg, and H. J. W. De Baar (2015), Zonal distribution of dissolved aluminium in the Mediterranean Sea, *Mar. Chem.*, *177*, 87–100.
Rudnick, R. L., and S. Gao (2003), Composition of the continental crust, *Treatise Geochem.*, *3*, 1–64.
Saito, M. A., and J. W. Moffett (2001), Complexation of cobalt by natural organic ligands in the Sargasso Sea as determined by a new high-sensitivity electrochemical cobalt speciation method suitable for open ocean work, *Mar. Chem.*, *75*(1), 49–68.
Saito, M. A., and J. W. Moffett (2002), Temporal and spatial variability of cobalt in the Atlantic Ocean, *Geochim. Cosmochim. Acta*, *66*, 1943–1953.
Saito, M. A., J. W. Moppett, S. W. Chisholm, and J. B. Waterbury (2002), Cobalt limitation and uptake in *Prochlorococcus*, *Limnol. Oceanogr.*, *47*(6), 1629–1636.
Saito, M. A., T. J. Goepfert, A. E. Noble, E. M. Bertrand, P. N. Sedwick, and G. R. DiTullio (2010), A seasonal study of dissolved cobalt in the Ross Sea, Antarctica: Micronutrient behavior, absence of scavenging, and relationships with Zn, Cd, and P, *Biogeosciences*, *7*(12), 4059–4082.
Sanchez-Vidal, A., A. Calafat, M. Canals, J. Frigola, and J. Fabres (2005), Particle fluxes and organic carbon balance across the Eastern Alboran Sea (SW Mediterranean Sea), *Cont. Shelf Res.*, *25*(5), 609–628.
Sañudo-Wilhelmy, S. A., A. B. Kustka, C. J. Gobler, D. A. Hutchins, M. Yang, K. Lwiza, J. Burns, D. G. Capone, J. A. Raven, and E. J. Carpenter (2001), Phosphorus limitation of nitrogen fixation by *Trichodesmium* in the central Atlantic Ocean, *Nature*, *411*(6833), 66–69.
Sañudo-Wilhelmy, S. A., C. J. Gobler, M. Okbamichael, and G. T. Taylor (2006), Regulation of phytoplankton dynamics by vitamin B12, *Geophys. Res. Lett.*, *33*, L04604, doi:10.1029/2005GL025046.
Schmitz, W. J., and M. S. McCartney (1993), On the north Atlantic circulation, *Rev. Geophys.*, *31*, 29–49, doi:10.1029/92RG02583.
Shelley, R. U., et al. (2012), Controls on dissolved cobalt in surface waters of the Sargasso Sea: Comparisons with iron and aluminum, *Global Biogeochem. Cycles*, *26*, GB2020, doi:10.1029/2011GB004155.
Soto-Navarro, J., F. Criado-Aldeanueva, J. García-Lafuente, and A. Sánchez-Román (2010), Estimation of the Atlantic inflow through the Strait of Gibraltar from climatological and in situ data, *J. Geophys. Res.*, *115*, C10023, doi:10.1029/2010JC006302.
Speicher, E. A., et al. (2006), Particulate organic carbon export fluxes and size-fractionated POC/234 Th ratios in the Ligurian, Tyrrhenian and Aegean Seas, *Deep Sea Res., Part I*, *53*(11), 1810–1830.
Struglia, M. V., A. Mariotti, and A. Filograsso (2004), River discharge into the Mediterranean Sea: Climatology and aspects of the observed variability, *J. Clim.*, *17*(24), 4740–4751.
Sunda, W. G., and S. A. Huntsman (1995), Cobalt and zinc inter-replacement in marine phytoplankton: Biological and geochemical implications, *Limnol. Oceanogr.*, *40*, 1404–1417.
Tankere, S. P. C. (1998), The biogeochemistry of some trace metals in some eutrophic areas: The Adriatic Sea and the North-western Black Sea, Doctoral dissertation, Univ. of Southampton.
Tovar-Sánchez, A., S. A. Sanudo-Wilhelmy, A. B. Kustka, S. Agusti, J. Dachs, D. A. Hutchins, D. G. Capone, and C. M. Duarte (2006), Effects of dust deposition and river discharges on trace metal composition of *Trichodesmium* spp. in the tropical and subtropical North Atlantic Ocean, *Limnol. Oceanogr.*, *51*(4), 1755–1761.
Tovar-Sánchez, A., J. M. Arrieta, C. M. Duarte, and S. A. Sañudo-Wilhelmy (2014), Spatial gradients in trace metal concentrations in the surface microlayer of the Mediterranean Sea, *Front. Mar. Sci.*, *1*, 79.
Tsuchiya, M., L. D. Talley, and M. S. McCartney (1992), An eastern Atlantic section from Iceland southward across the equator, *Deep Sea Res. Part A*, *39*(11), 1885–1917.
Twining, B. S., and S. B. Baines (2013), The trace metal composition of marine phytoplankton, *Annu. Rev. Mar. Sci.*, *5*, 191–215.
Twining, B. S., S. B. Baines, J. B. Bozard, S. Vogt, E. A. Walker, and D. M. Nelson (2011), Metal quotas of plankton in the equatorial Pacific Ocean, *Deep Sea Res., Part II*, *58*(3), 325–341.
Twining, B. S., S. D. Nodder, A. L. King, D. A. Hutchins, G. R. LeCleir, J. M. DeBruyn, W. Maas Elizabeth, S. Vogt, S. W. Wilhelm, and P. W. Boyd (2014), Differential remineralization of major and trace elements in sinking diatoms, *Limnol. Oceanogr.*, *59*(3), 689–704.
Twining, B. S., S. Rauschenberg, P. L. Morton, and S. Vogt (2015), Metal contents of phytoplankton and labile particulate material in the North Atlantic Ocean, *Prog. Oceanogr.*, *137*, 261–283.
van Aken, H. M. (2000a), The hydrography of the mid-latitude northeast Atlantic Ocean: I: The deep water masses, *Deep Sea Res., Part I*, *47*(5), 757–788.
van Aken, H. M. (2000b), The hydrography of the mid-latitude Northeast Atlantic Ocean: II: The intermediate water masses, *Deep Sea Res., Part I*, *47*(5), 789–824.
van Cappellen, P., H. R. Powley, K. C. Emeis, and M. D. Krom (2014), A biogeochemical model for phosphorus and nitrogen cycling in the Eastern Mediterranean Sea: Part 1. Model development, initialization and sensitivity, *J. Mar. Syst.*, *139*, 460–471.
van de Poll, W. H., P. G. Boute, P. D. Rozema, A. G. J. Buma, G. Kulk, and M. J. A. Rijkenberg (2015), Sea surface temperature control of taxon specific phytoplankton production along an oligotrophic gradient in the Mediterranean Sea, *Mar. Chem.*, *177*, 536–544.
van Geen, A., P. Rosener, and E. Boyle (1988), Entraînaient of trace-metal-enriched Atlantic shelf water in the inflow to the Mediterranean Sea, *Nature*, *331*, 4.
van Geen, A., E. A. Boyle, and W. S. Moore (1991), Trace metal enrichments in waters of the Gulf of Cadiz, Spain, *Geochim. Cosmochim. Acta*, *55*(8), 2173–2191.
Van Geen, A., J. F. Adkins, E. A. Boyle, C. H. Nelson, and A. Palanques (1997), A 120-yr record of widespread contamination from mining of the Iberian pyrite belt, *Geology*, *25*(4), 291–294.
Vega, M., and C. M. G. van den Berg (1997), Determination of cobalt in seawater by catalytic adsorptive cathodic stripping voltammetry, *Anal. Chem.*, *69*(5), 874–881.
Wu, P., and K. Haines (1998), The general circulation of the Mediterranean Sea from a 100 year simulation, *J. Geophys. Res.*, *103*, 1121–1135, doi:10.1029/97JC02720.

Yee, D., and F. M. Morel (1996), In vivo substitution of zinc by cobalt in carbonic anhydrase of a marine diatom, *Limnol. Oceanogr.*, *41*(3), 573–577.

Zervakis, V., D. Georgopoulos, A. P. Karageorgis, and A. Theocharis (2004), On the response of the Aegean Sea to climatic variability: A review, *Int. J. Climatol.*, *24*(14), 1845–1858.

Zhang, H., R. Wollast, J. C. Vire, and G. J. Patriarche (1989), Simultaneous determination of cobalt and nickel in sea water by adsorptive cathodic stripping square-wave voltammetry, *Analyst*, *114*(12), 1597.